AD-A053 312 ARMY ELECTRONICS RESEARCH AND DEVELOPMENT COMMAND WS--ETC F/G 4/1
THE 1979 SOLAR ECLIPSE AND VALIDATION OF D-REGION MODELS.(U)
MAR 78 M G HEAPS

UNCLASSIFIED ERADCOM/ASL-TR-0002 NL

1 OF 1
AD A053312

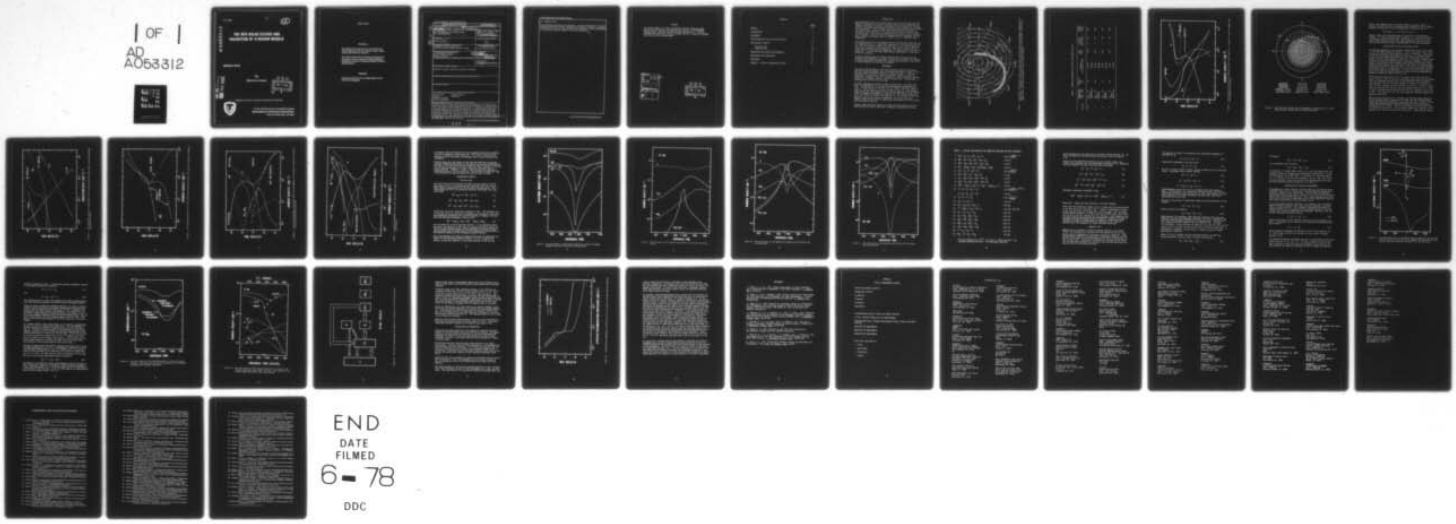

END
DATE FILMED
6-78
DDC

ASL-TR-0002

(12)

THE 1979 SOLAR ECLIPSE AND VALIDATION OF D-REGION MODELS

MARCH 1978

By

Melvin G. Heaps

Approved for public release; distribution unlimited.

US Army Electronics Research and Development Command
Atmospheric Sciences Laboratory
White Sands Missile Range, N.M. 88002

NOTICES

Disclaimers

The findings in this report are not to be construed as an official Department of the Army position, unless so designated by other authorized documents.

The citation of trade names and names of manufacturers in this report is not to be construed as official Government indorsement or approval of commercial products or services referenced herein.

Disposition

Destroy this report when it is no longer needed. Do not return it to the originator.

SECURITY CLASSIFICATION OF THIS PAGE *(When Data Entered)*

REPORT DOCUMENTATION PAGE

READ INSTRUCTIONS BEFORE COMPLETING FORM

1. REPORT NUMBER: ~~ASL-TR-0002~~ ERADCOM/ASL-TR-0002
2. GOVT ACCESSION NO.
3. RECIPIENT'S CATALOG NUMBER

4. TITLE *(and Subtitle)*: THE 1979 SOLAR ECLIPSE AND VALIDATION OF D-REGION MODELS
5. TYPE OF REPORT & PERIOD COVERED: R&D Technical Report
6. PERFORMING ORG. REPORT NUMBER

7. AUTHOR(s): Melvin G. Heaps
8. CONTRACT OR GRANT NUMBER(s)

9. PERFORMING ORGANIZATION NAME AND ADDRESS: Atmospheric Sciences Laboratory, White Sands Missile Range, New Mexico 88002
10. PROGRAM ELEMENT, PROJECT, TASK AREA & WORK UNIT NUMBERS: DA Task No. 1L162111AH71

11. CONTROLLING OFFICE NAME AND ADDRESS: US Army Electronics Research and Development Command, Adelphi, MD 20783
12. REPORT DATE: Mar[illegible]78
13. NUMBER OF PAGES: 39 (12 38 p.)

14. MONITORING AGENCY NAME & ADDRESS *(if different from Controlling Office)*
15. SECURITY CLASS. *(of this report)*: UNCLASSIFIED
15a. DECLASSIFICATION/DOWNGRADING SCHEDULE

16. DISTRIBUTION STATEMENT *(of this Report)*

Approved for public release; distribution unlimited.

17. DISTRIBUTION STATEMENT *(of the abstract entered in Block 20, if different from Report)*

18. SUPPLEMENTARY NOTES

19. KEY WORDS *(Continue on reverse side if necessary and identify by block number)*

Solar eclipse
D-region
Electron attachment
Electron detachment
Electron density
Ionization

20. ABSTRACT *(Continue on reverse side if necessary and identify by block number)*

The 26 February 1979 solar eclipse provides an opportunity for controlled experiments to help differentiate among the several processes of D-region ionization. One major concern is whether the sources of ionization are largely solar or predominantly due to particle precipitation. Of equal importance are the electron attachment and detachment processes which determine the free electron densities. Comparisons of current gas-phase ion chemistry calculations with scattered available data show serious discrepancies for electron density variations above 70 km. The inclusion of a new class of reactions involving aerosols

→ next page

DD FORM 1 JAN 73 1473 EDITION OF 1 NOV 65 IS OBSOLETE

SECURITY CLASSIFICATION OF THIS PAGE *(When Data Entered)*

410 663

20. ABSTRACT (cont)

or particulates would seem to be indicated. A correct determination of D-region electron densities and electron attachment and detachment processes is necessary for proper utilization of Army communications systems and a better understanding of the effects of nuclear weapons in the middle atmosphere.

PREFACE

The author thanks D. W. Hoock of Physical Sciences Laboratory, New Mexico State University, for computational support of the DAIRCHEM computer code. The many helpful conversations with Drs. L. Hale of Pennsylvania State and F. E. Niles of ASL, and Mr. R. Sears of Lockheed, Palo Alto, are also acknowledged.

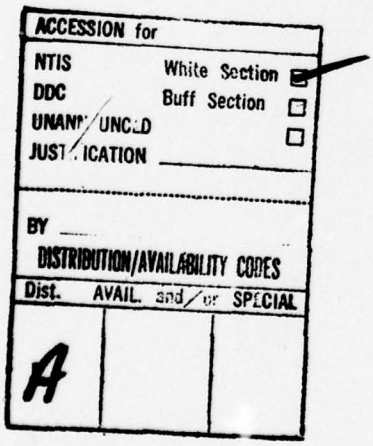

CONTENTS

INTRODUCTION

The 26 February 1979 solar eclipse, the last one visible from the North American Continent this century, provides opportunity to determine the effects of different sources of ionization on the D-region and to study electron attachment and detachment processes which determine the D-region electron density. Solar eclipses have the advantage of providing a day-"night"-day transition on the time scale of several minutes, thus allowing study of the rapid ion chemistry while assuring that transport can be ignored. The bulk neutral atmosphere remains unchanged, and the minor neutral constituents vary in a manner which is reasonably well understood.

The purpose here will be to determine what the background conditions are at a selected (but still tentative) experimental site along the path of the 1979 eclipse and to predict the expected electron and ion densities according to currently known chemistry. Comparison is made with previous solar eclipse data, and suggestions for new physical processes are presented. A list of desirable experimental measurements is also compiled as an appendix.

A correct determination of D-region electron densities and electron attachment and detachment processes is necessary for proper utilization of Army communications systems and a better understanding of the effects of nuclear weapons in the middle atmosphere.

BACKGROUND

The path of the 26 February 1979 solar eclipse crosses North America from the Oregon-Washington coast up through Hudson Bay as shown in Fig. 1. The more readily accessible sites are listed in Table 1. The less populated areas are sites 4 and 6 in northern Montana and south of Hudson Bay. Logistics are more favorable for site 4 at Poplar, Montana, located on US Highway 2 and on a major railroad line. Calculations presented here will be for this site.

The model atmosphere utilized in these calculations is the CIRA 1972 March 1 atmosphere for 50° N, with the corresponding temperature profile. The H_2O content is nominally set at 5 ppm of the total neutral density. The NO profile is similar to that of Meira [1] with somewhat lower values near the minimum at 85 km and extrapolated to match the NO values of Ogawa and Shimazaki [2] near 50 km. The initial values of O and O_3 are taken from Ogawa and Shimazaki, but are allowed to establish dynamical equilibrium values corresponding to current conditions. Figure 2 shows the profiles of these minor constituents at first contact and later during totality.

Figure 3 shows the major regions of proton and hard electron particle precipitation and the eclipse path in magnetic coordinates and time.

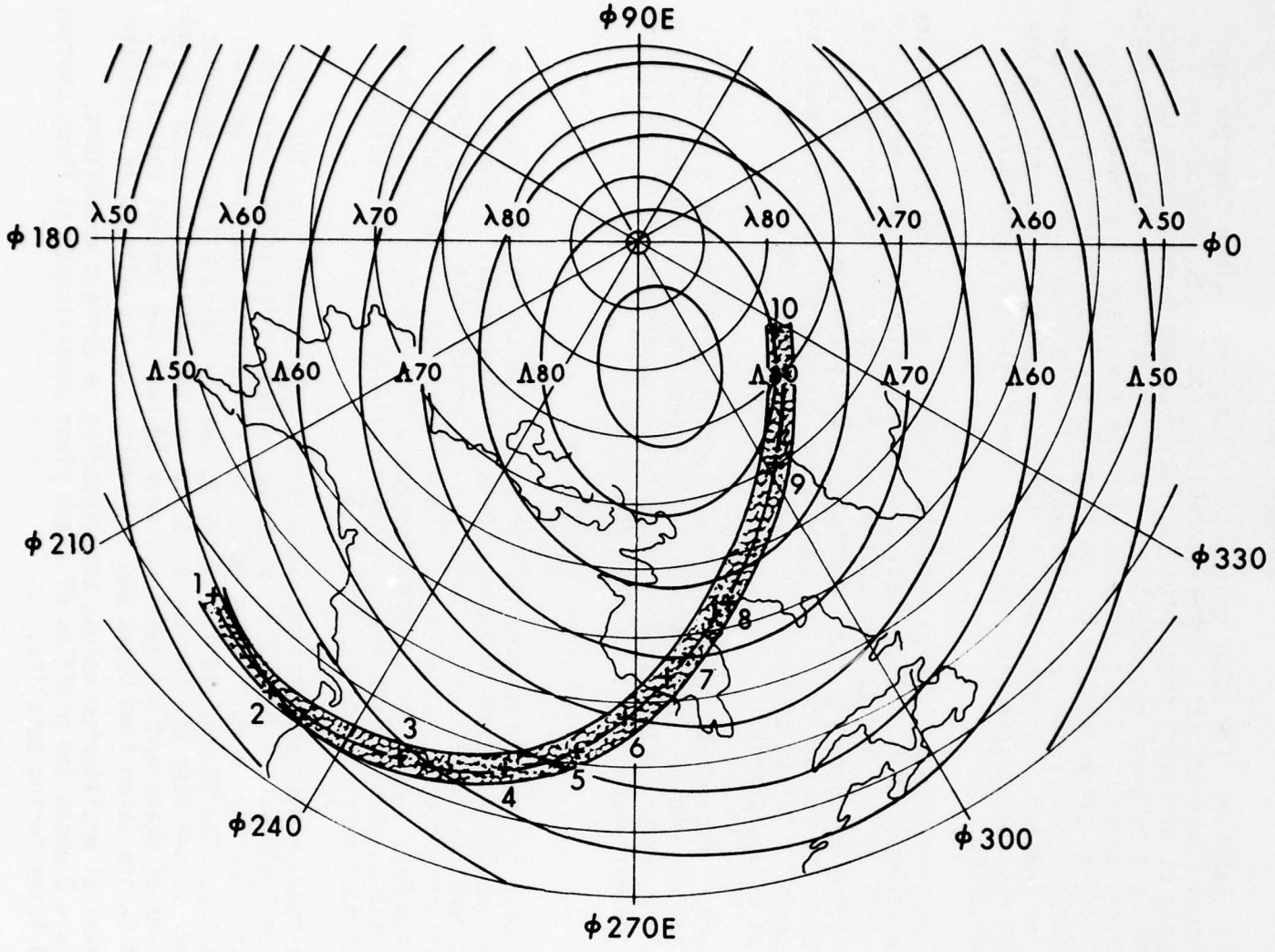

Figure 1. The path of the 26 Feb 79 solar eclipse across the North American continent; shadow width is approximate. Geomagnetic latitudes have been superimposed on the geographic coordinates. Numbers along the path correspond to sites listed in Table 1.

TABLE 1. READILY ACCESSIBLE SITES OF 1979 SOLAR ECLIPSE

Site No.	Geographic Long (°W)	Geographic Lat (°N)	Magnetic Lat (°)	Ephemeris (and Local Time)	Sun Angle (°)	Eclipse Duration (min)	Eclipse Duration (sec)	Shadow Width (km)
2-3	121	46 (South Washington)	52	16:18 (08:18)	13.0	2	18	274
4	105	48 (North Montana)	58	16:36 (09:36)	23.2	2	43	307
5	98	50 (South Mantoba)	61	16:48 (10:48)	25.4	2	48	304
6	92	53 (South Hudson Bay)	65	17:00 (11:00)	25.5	2	48	292

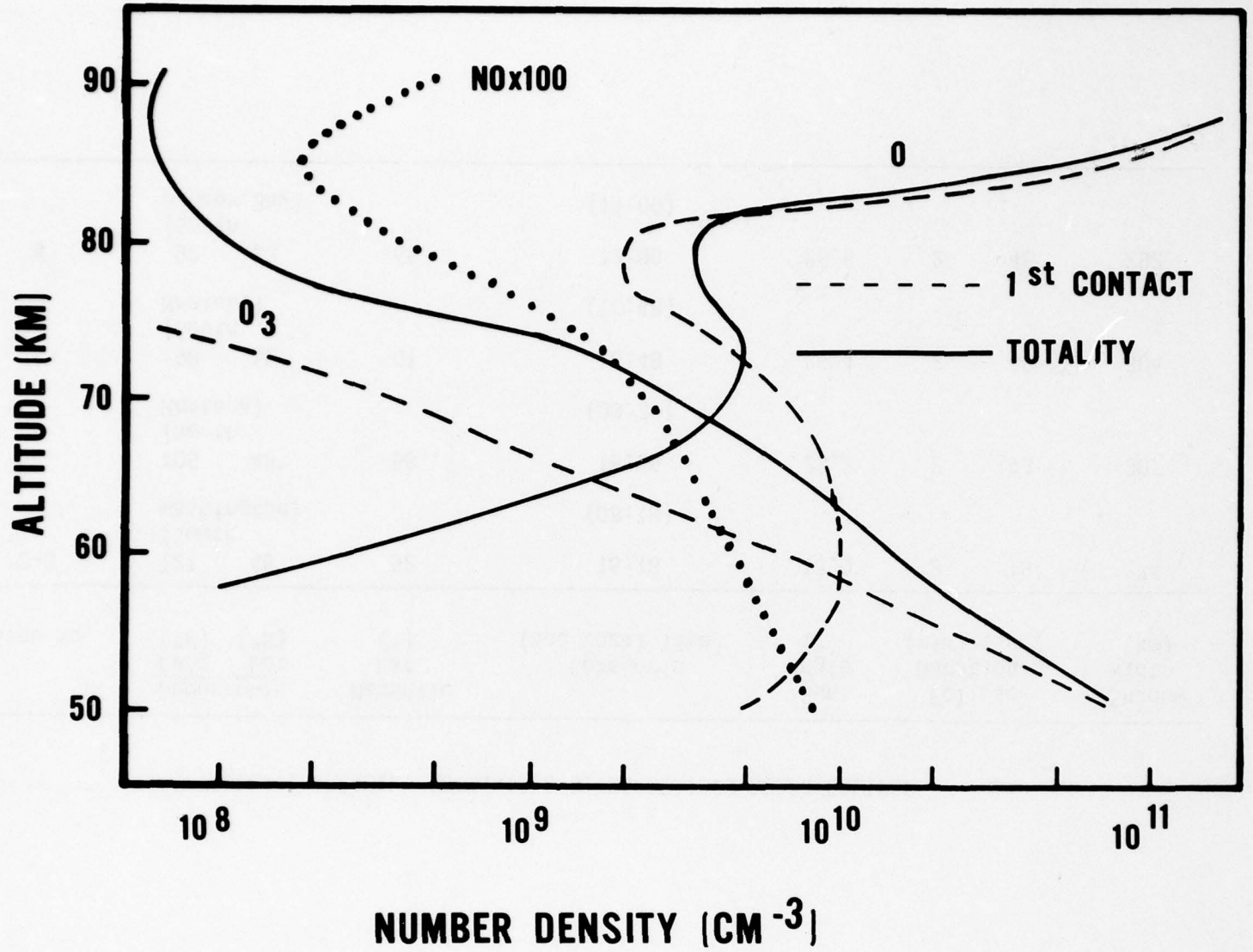

Figure 2. The number densities of the important minor constituents O, O_3 and NO. O and O_3 change from first contact to totality.

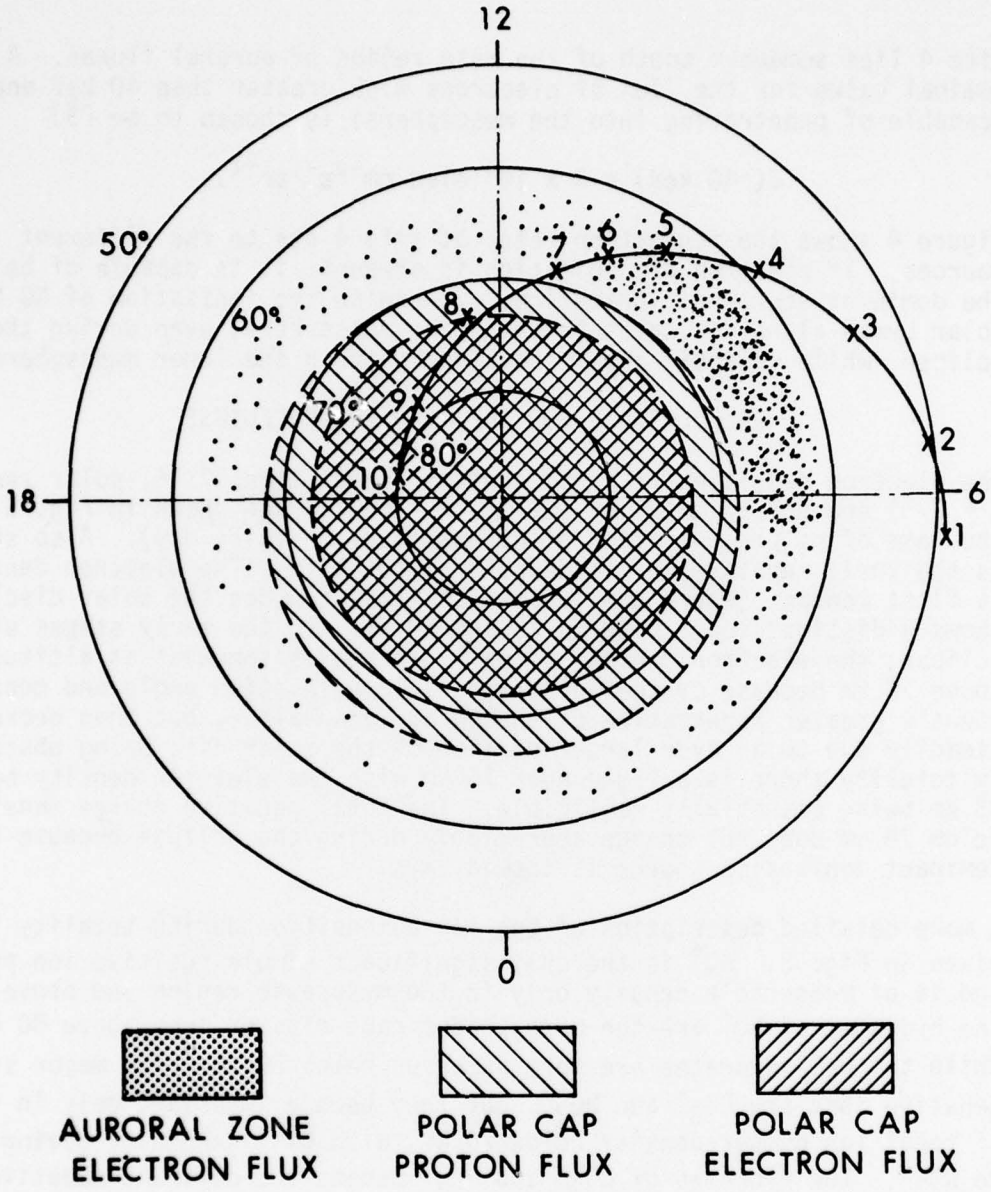

Figure 3. The 1979 solar eclipse path in geomagnetic coordinates as it intersects the main regions of particle precipitation.

Site 4 lies somewhat south of the main region of auroral fluxes. A nominal value for the flux of electrons with greater than 40 keV energy (capable of penetrating into the mesosphere) is chosen to be [3]

$$J(>40 \text{ keV}) = 3 \times 10^3 \text{ elec cm}^{-2}\text{s}^{-1}\text{sr}^{-1}.$$

Figure 4 shows the ionization rates at site 4 due to the different sources. If electron precipitation is present, it is capable of being the dominant source of ionization. Otherwise the ionization of NO by solar Lyman-alpha dominates in the upper mesosphere, even during the eclipse, while galactic cosmic rays dominate in the lower mesosphere.

CALCULATIONS FOR THE 1979 SOLAR ECLIPSE

The electron densities at first contact (local time 07:16, solar zenith $\chi = 77°$) and during totality (09:36, $\chi = 66.7°$) are shown in Fig. 5 for the case of no precipitating electrons (i.e., a quiet day). Also shown is the total negative charge density at totality. The electron density at first contact (where the lunar disc first touches the solar disc) shows a distinct ledge between 75 and 80 km. In the early stages of the eclipse, the electron density actually increases somewhat at altitudes above 70 km because of the increasing solar elevation angle and consequently greater penetration of the solar Lyman-alpha, but then decreases steadily due to an ever larger portion of the solar disc being obscured. By totality there is a ledge near 75 km with the electron density below 65 km being essentially negligible. The total negative charge density below 70 km does not change appreciably during the eclipse because the dominant ionization source is cosmic rays.

A more detailed description of the ion composition during totality is given in Fig. 6. NO^+ is the only significant simple positive ion present and is of measurable density only in the mesopause region and above. The hydrates of NO^+ are the more predominant cluster ions above 80 km, while the H_3O^+ hydrates are more numerous below 80 km. The major simple negative ions are CO_3^- and NO_3^-, but they become important only in terms of total ion number density below 70 km, with CO_3^- gradually giving way to NO_3^-. The hydrates of CO_3^- and NO_3^- become the dominant negative ion species below 65 km.

When electron precipitation is included, the absolute number densities of the ionized species increase at all times, but the relative proportions stay very much the same as in the quiet day case. Figure 7 illustrates the charged particle densities during totality when electron precipitation is included. The main differences occur in the positive ion chemistry above 80 km. The switchover between H_3O^+ hydrates and NO^+ hydrates still occurs at 80 km, but now the $NO^+ \cdot (H_2O)n$ density begins

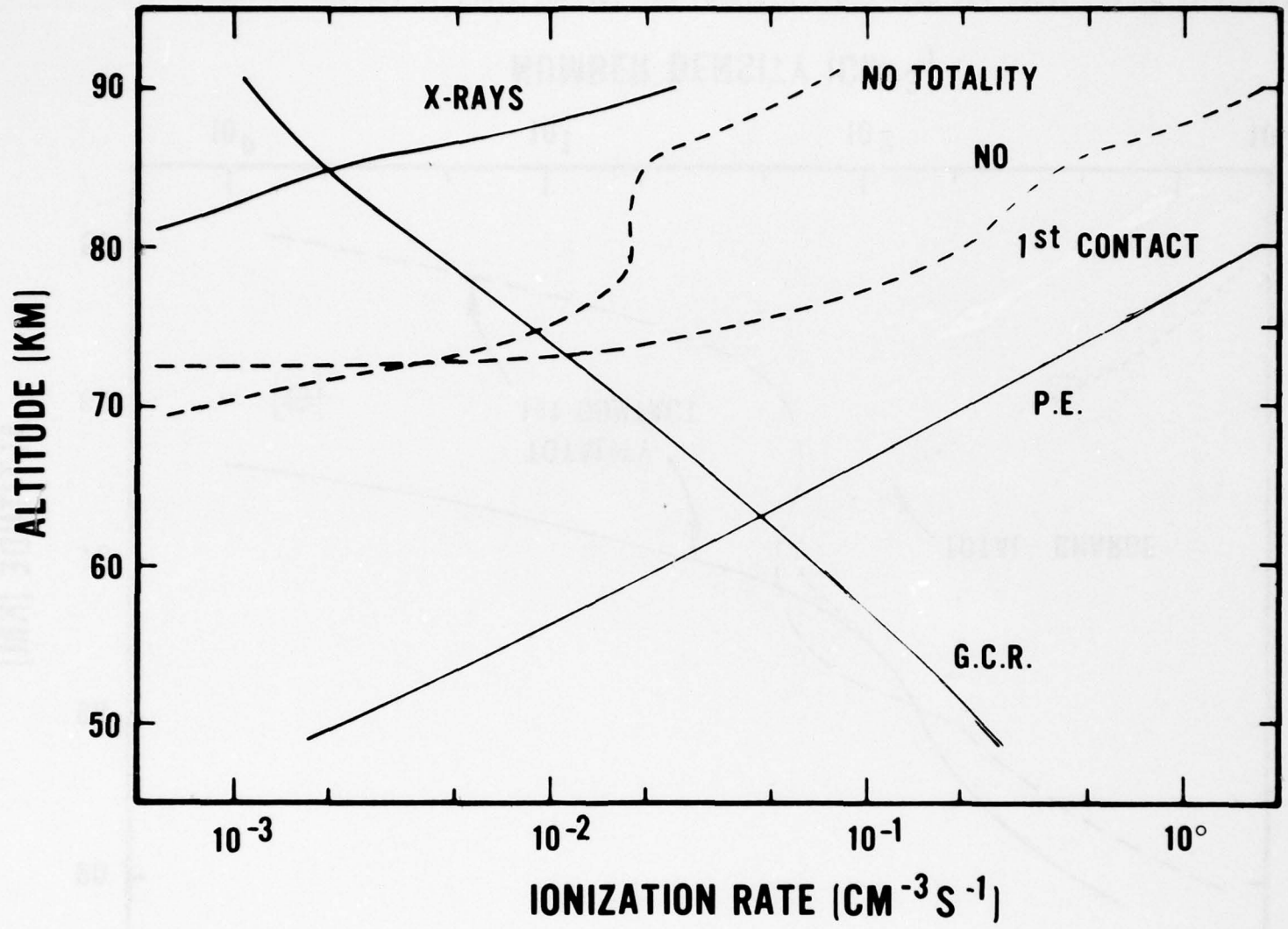

Figure 4. The ionization rates of Lyman-alpha on NO, X-rays, galactic cosmic rays, and precipitating electrons at site 4.

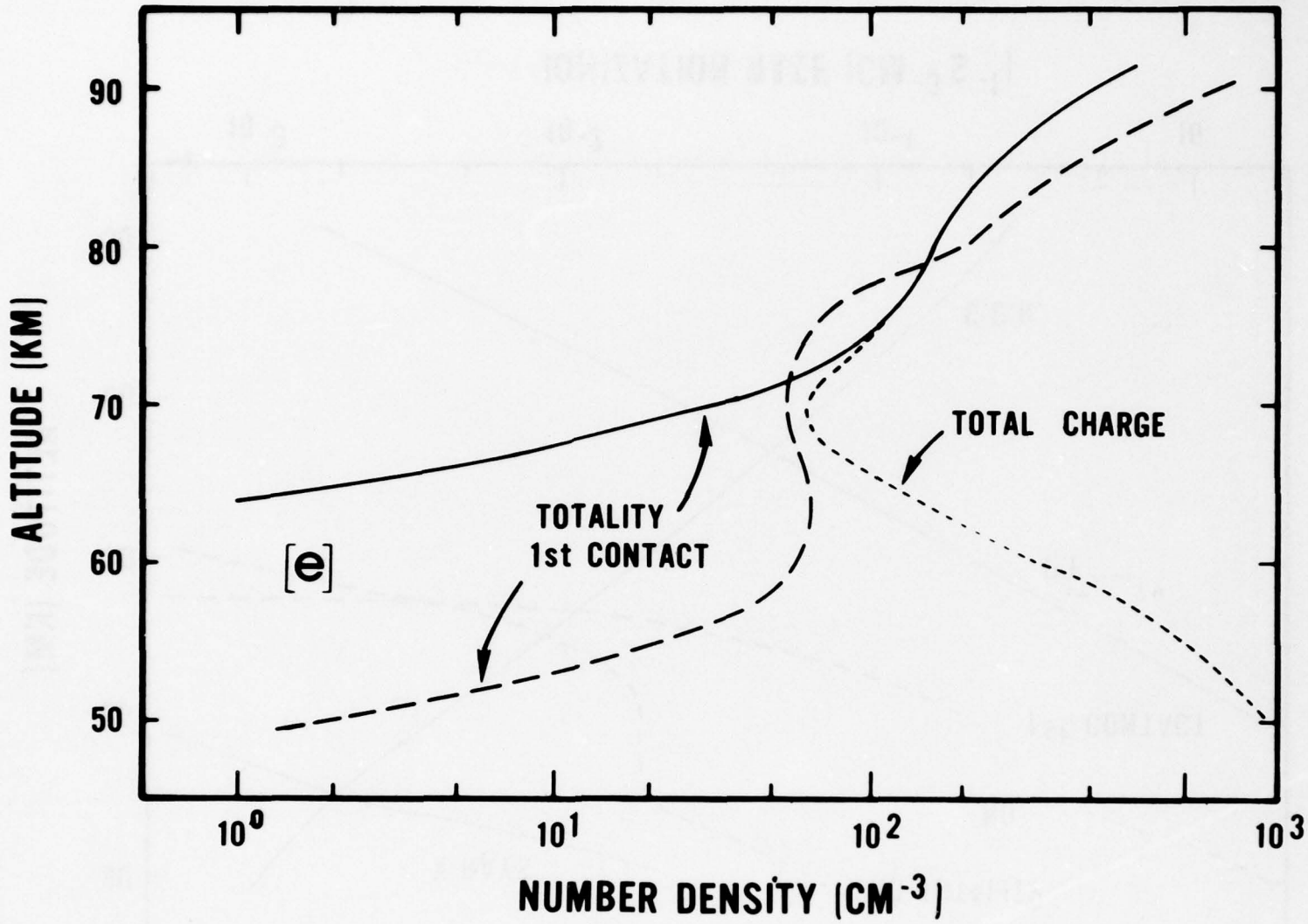

Figure 5. The electron densities at first contact and totality along with the total charge at totality.

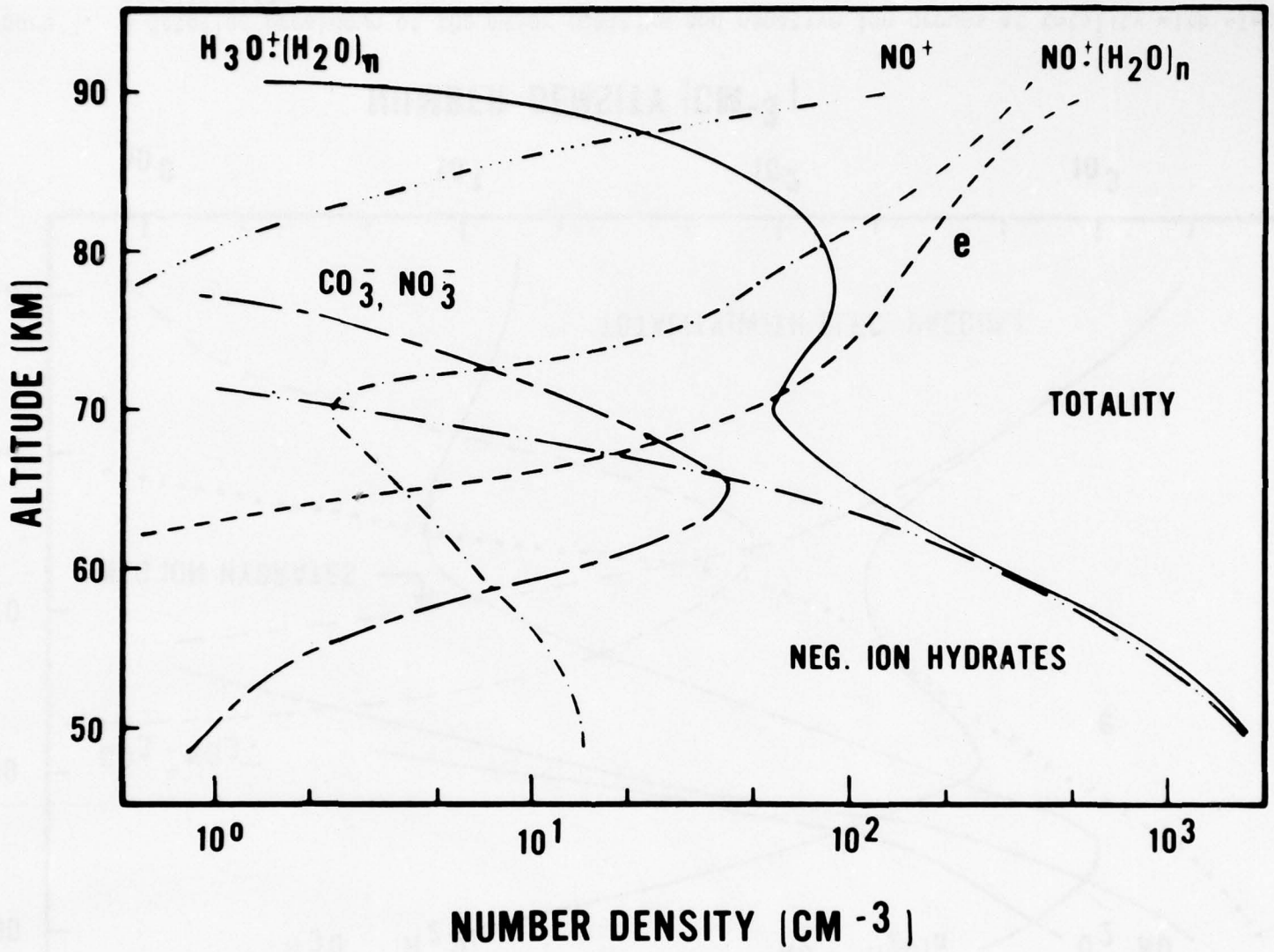

Figure 6. A detailed breakdown of the major positive and negative ion groups at totality for site 4 with no electron precipitation.

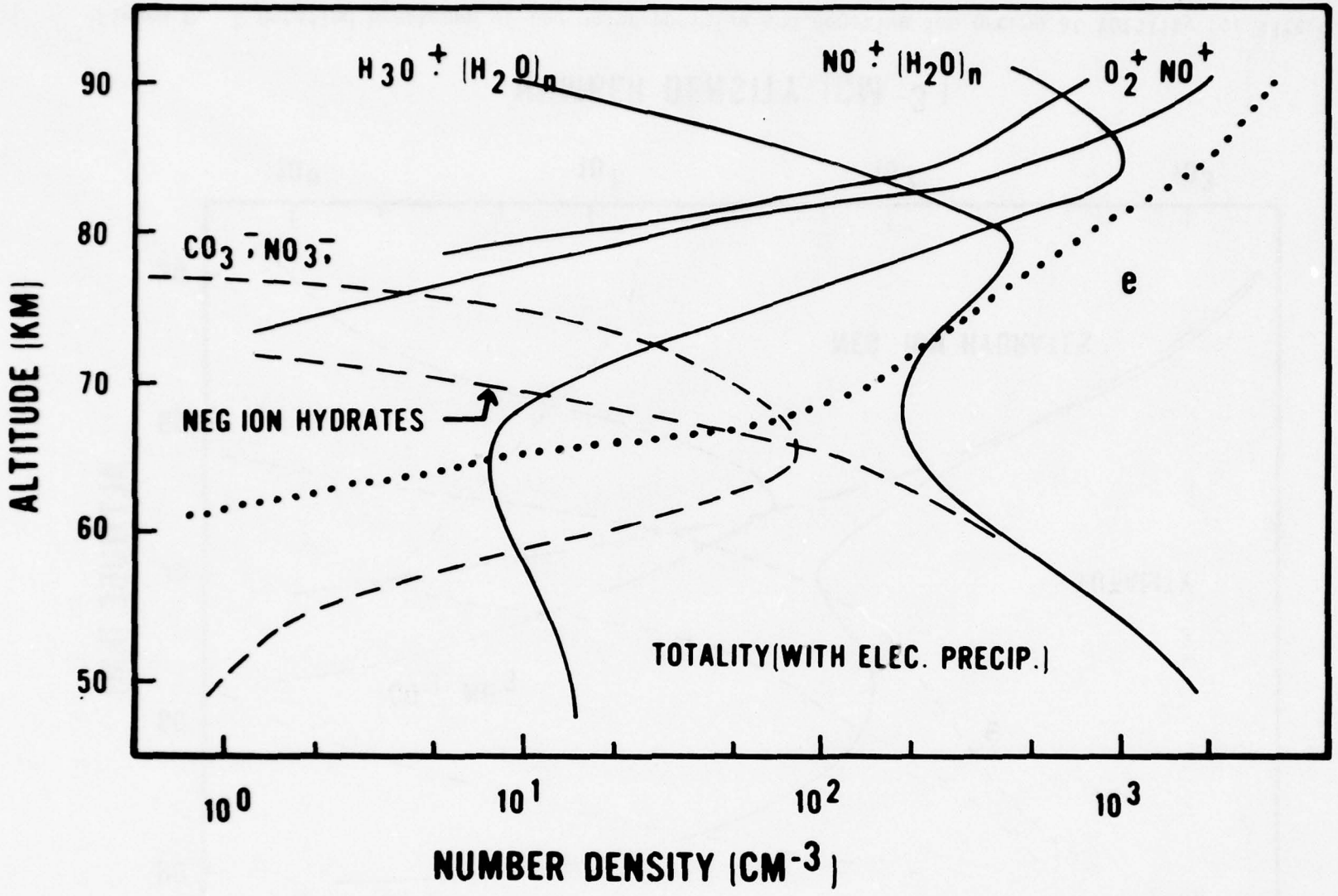

Figure 7. A detailed breakdown of the major positive and negative ion groups at totality with electron precipitation.

to decrease above 85 km because of the increased electron-ion recombination due to enhanced electron densities. NO^+ and O_2^+ become the predominant positive ions above the mesopause when electron precipitation is present.

Figure 8 gives the time history of the electron densities at selected altitudes between 50 and 80 km for the case of no electron precipitation. Totality is at 16:36 UT (09:36 local time) and lasts 2 minutes 43 seconds; for the time period shown, at least a portion of the solar disc is always obscured. Figures 9, 10 and 11 show the detailed histories of the negative ions at 70, 65, and 60 km. The positive ion densities show little variation at these altitudes and have not been included.

DISCUSSION OF RESULTS

Positive Ions

The main flow along the positive ion chain, the end results of which were shown in Fig. 6, is through the NO^+ hydration chain for the case where particle precipitation is not the major ionizing source. The faster paths are felt to be switching reactions (see Table 2 for reaction rates)

$$NO^+ + N_2 + M \rightarrow NO^+ \cdot N_2 + M \,, \qquad (1)$$

$$NO^+ \cdot N_2 + CO_2 \rightarrow NO^+ \cdot CO_2 + N_2 \,, \qquad (2)$$

$$NO^+ \cdot CO_2 + H_2O \rightarrow NO^+ \cdot H_2O + CO_2 \,, \qquad (3)$$

rather than the direct three-body attachment of H_2O. The analogous set of reactions (with the same set of estimated rate constants) occurs with each subsequent hydration until the third hydrate is reached. At this point the two-body attachment of water yields

$$NO^+ \cdot (H_2O)_3 + H_2O \rightarrow H_3O^+ \cdot (H_2O)_2 + HNO_2 \,, \qquad (4)$$

and the hydronium ion chain has been entered. In the mesopause region and above, the hydration of NO^+ does not proceed efficiently beyond the first or second hydrate because of the decreasing efficiency of three-body processes and the larger electron-ion recombination coefficients of the hydrates coupled with the increasing electron density.

Below the mesopause the rapidly increasing efficiency of three-body processes and the decreasing electron density, plus the increasing NO density, allows the formation of the higher hydrates of NO^+ and the

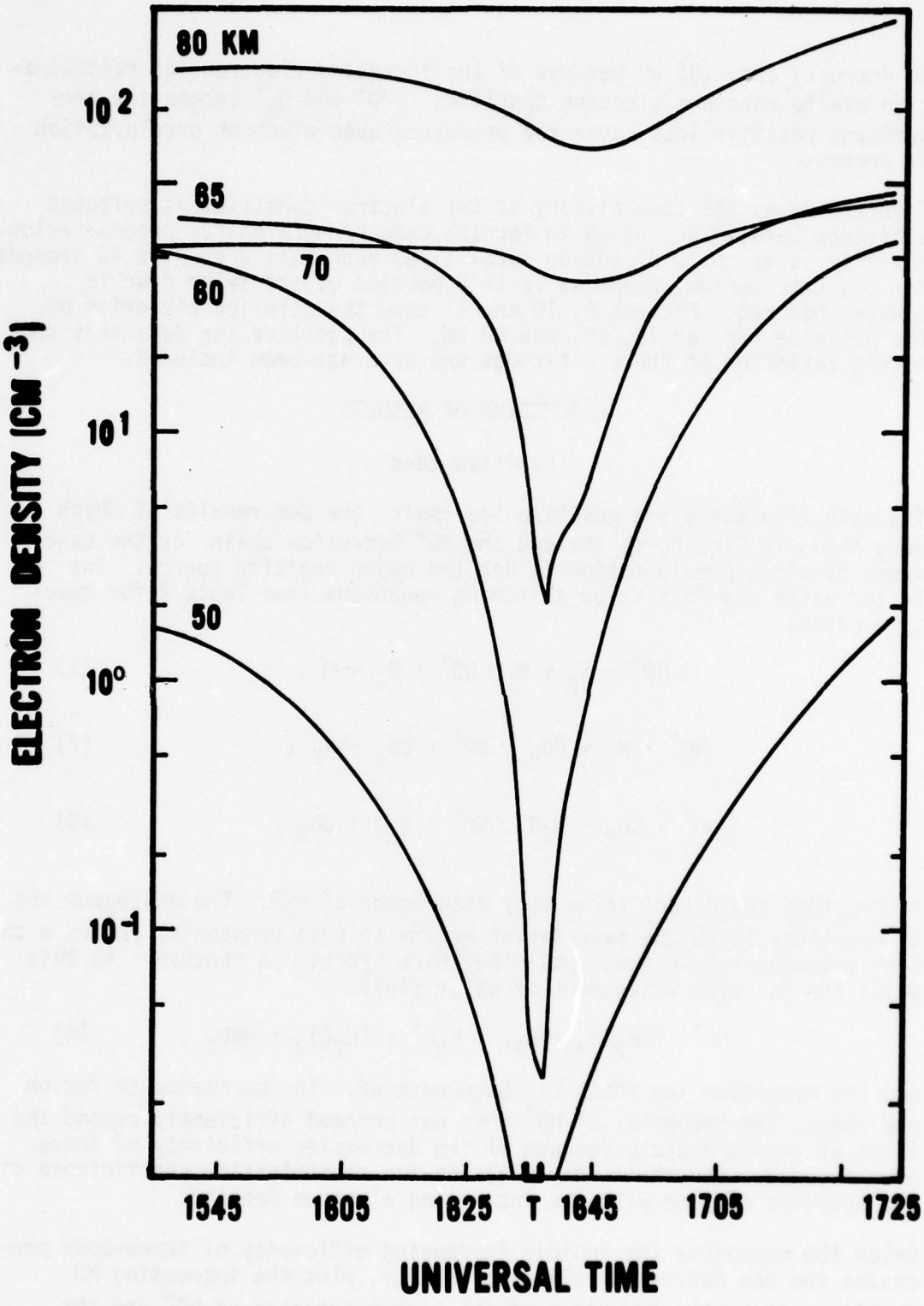

Figure 8. The time history of the electron density for specific altitudes between 50 and 80 km during the eclipse period.

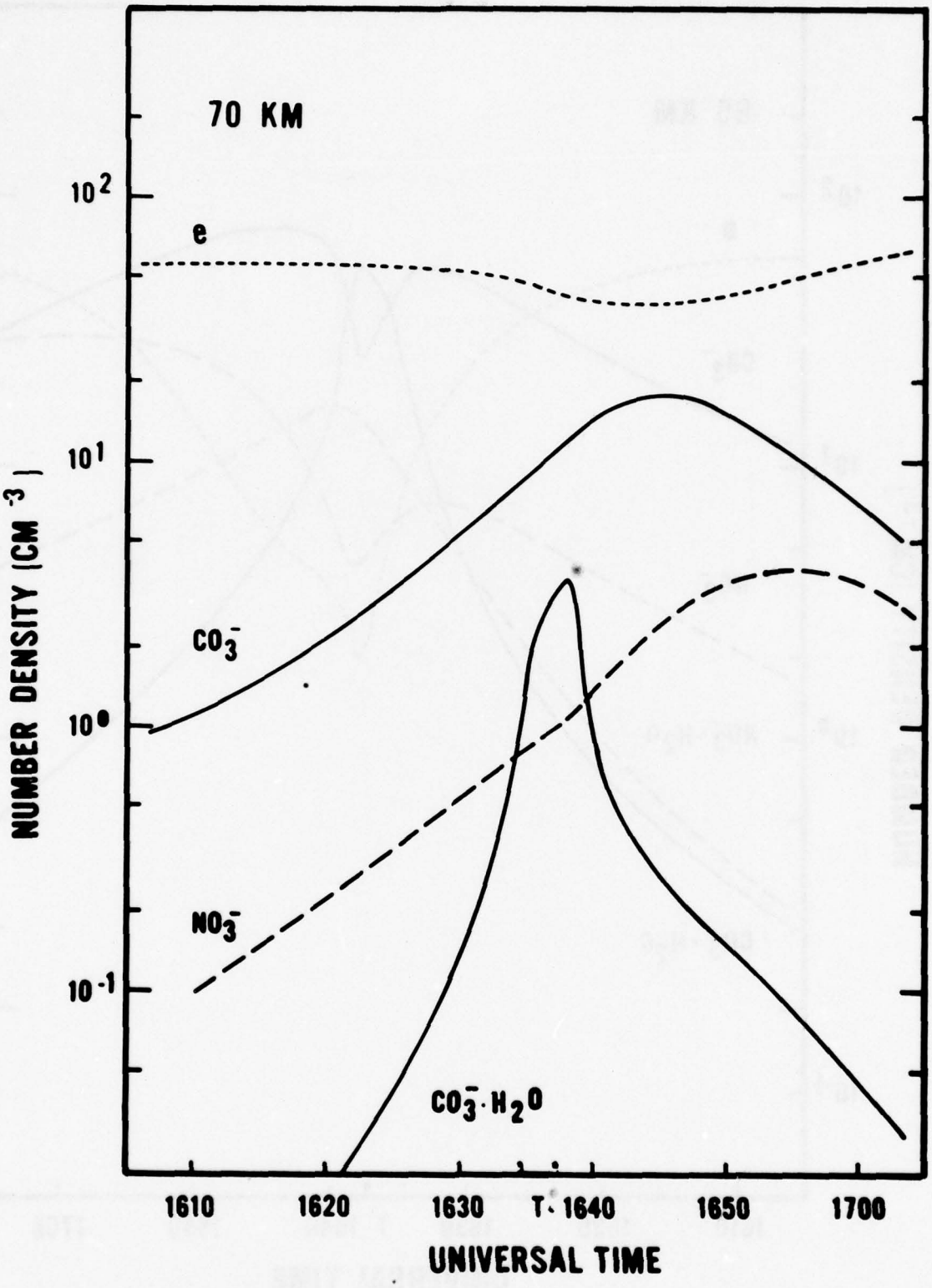

Figure 9. The time history of the negative ion species at 70 km during the eclipse period.

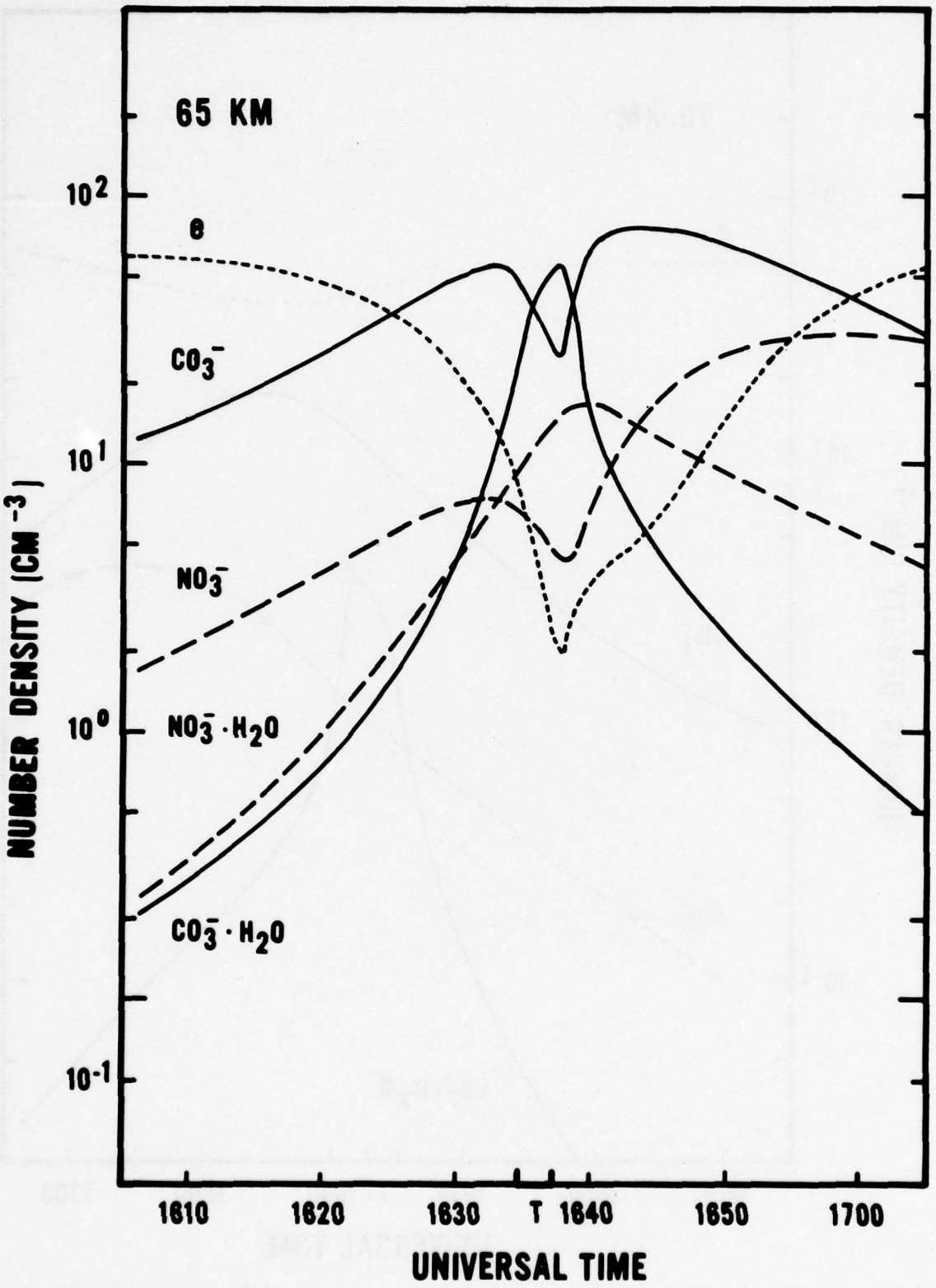

Figure 10. The time history of the negative ion species at 65 km during the eclipse period.

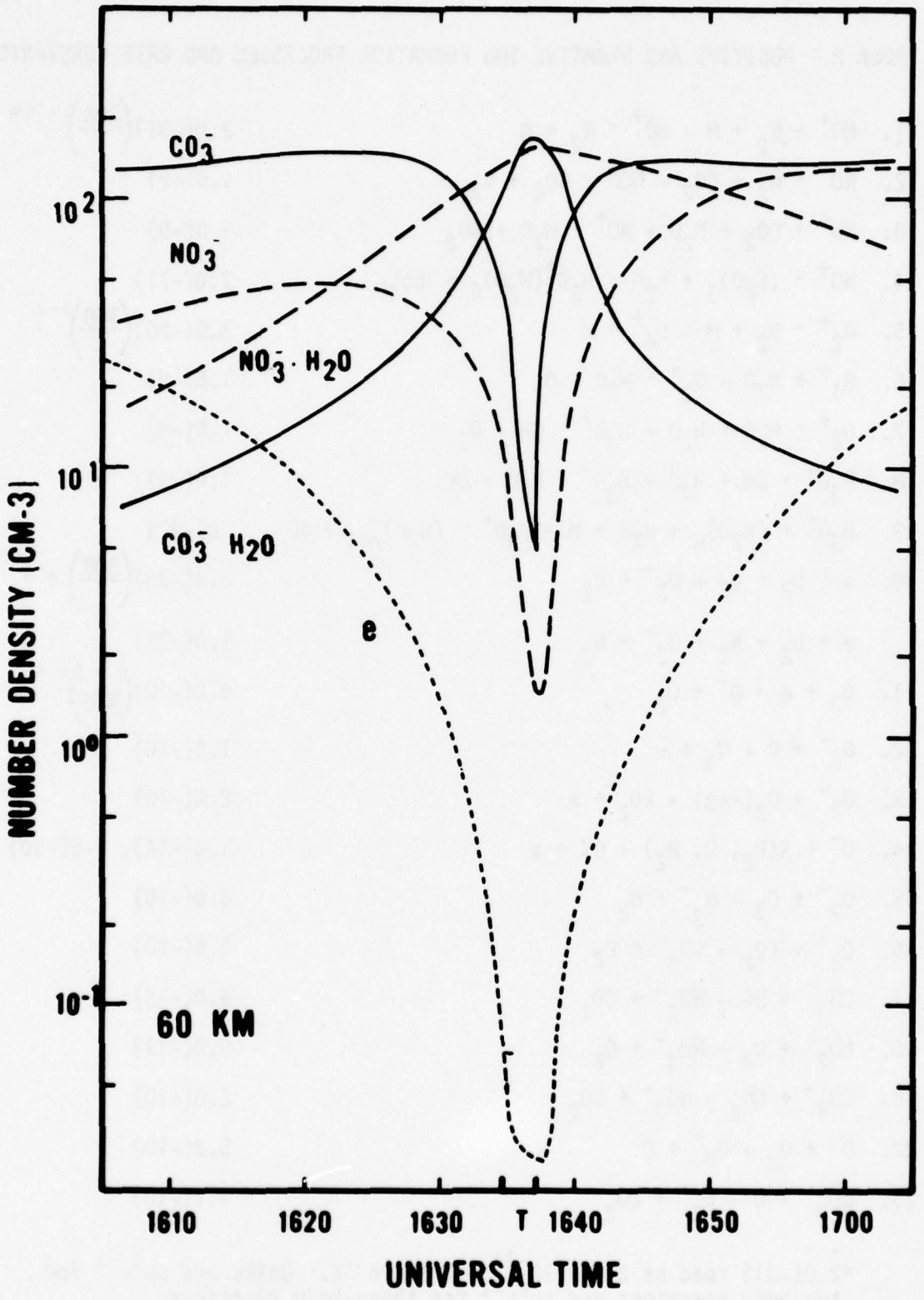

Figure 11. The time history of the negative ion species at 60 km during the eclipse period.

TABLE 2. POSITIVE AND NEGATIVE ION FORMATION PROCESSES AND RATE CONSTANTS

1.	$NO^+ + N_2 + M \rightarrow NO^+ \cdot N_2 + M$	$2.0(-31)\left(\frac{300}{T}\right)^{4.4}$*
2.	$NO^+ \cdot N_2 + CO_2 \rightarrow NO^+ \cdot CO_2 + N_2$	1.0(-9)
3.	$NO^+ \cdot CO_2 + H_2O \rightarrow NO^+ \cdot H_2O + CO_2$	1.0(-9)
4.	$NO^+ \cdot (H_2O)_3 + H_2O \rightarrow H_3O^+(H_2O)_2 + HNO_2$	7.0(-11)
5.	$O_2^+ \cdot O_2 + M \rightarrow O_4^+ + M$	$3.9(-30)\left(\frac{300}{T}\right)^{3.2}$
6.	$O_4^+ + H_2O \rightarrow O_2^+ \cdot H_2O + O_2$	1.5(-9)
7.	$O_2^+ \cdot H_2O + H_2O \rightarrow H_3O^+ \cdot OH + O_2$	1.0(-9)
8.	$H_3O^+ \cdot OH + H_2O \rightarrow H_3O^+ \cdot H_2O + OH$	1.4(-9)
9.	$H_3O^+ \cdot (H_2O)_n + H_2O + M \rightarrow H_3O^+ \cdot (H_2O)_{n+1} + M$	~2(-27)
10.	$e + O_2 + O_2 \rightarrow O_2^- + O_2$	$1.4(-29)\left(\frac{300}{T}\right) e^{-(600/T)}$
	$e + O_2 + N_2 \rightarrow O_2^- + N_2$	1.0(-31)
11.	$O_3 + e \rightarrow O^- + O_2$	$9.0(-12)\left(\frac{T}{300}\right)^{1.5}$
12.	$O_2^- + O \rightarrow O_3 + e$	1.5(-10)
13.	$O_2^- + O_2(^1\Delta g) \rightarrow 2O_2 + e$	2.0(-10)
14.	$O^- + X(N_2, O, H_2) \rightarrow OX + e$	1.0(-14), 2-6(-10)
15.	$O_2^- + O_3 \rightarrow O_3^- + O_2$	6.0(-10)
16.	$O_3^- + CO_2 \rightarrow CO_3^- + O_2$	5.5(-10)
17.	$CO_3^- + NO \rightarrow NO_2^- + CO_2$	9.0(-12)
18.	$NO_2^- + O_3 \rightarrow NO_3^- + O_2$	9.0(-11)
19.	$CO_3^- + NO_2 \rightarrow NO_3^- + CO_2$	2.0(-10)
22.	$O^- + O_3 \rightarrow O_3^- + O$	5.3(-10)
23.	$CO_3^- + O \rightarrow O_2^- + CO_2$	1.1(-10)

*2.0(-31) read as 2.0×10^{-31}. T is in °K. Units are $cm^3 s^{-1}$ for two-body reactions and $cm^6 s^{-1}$ for three-body reactions.

rapid conversion to the hydronium ion hydrates through reaction (4). At 80 km the hydronium ions have become the dominant class of positive ions.

Below 75 km the background ionization due to galactic cosmic rays becomes more important than the Lyman-alpha ionization of NO. Hydronium ions are formed by the more direct and faster processes

$$O_2^+ + O_2 + M \rightarrow O_4^+ + M \ , \tag{5}$$

$$O_4^+ + H_2O \rightarrow O_2^+ \cdot H_2O + O_2 \ , \tag{6}$$

$$O_2^+ \cdot H_2O + H_2O \rightarrow H_3O^+ \cdot OH + O_2 \ , \tag{7}$$

$$H_3O^+ \cdot OH + H_2O \rightarrow H_3O^+ \cdot H_2O + OH \ . \tag{8}$$

Subsequent three-body attachment of H_2O

$$H_3O^+ \cdot (H_2O)n + H_2O + M \rightarrow H_3O^+ \cdot (H_2O)_{n+1} + M \tag{9}$$

makes $H_3O^+ \cdot (H_2O)_3$ the most prevalent of the H_3O^+ hydrates.

Under disturbed conditions (shown in Fig. 7) where particle precipitation is the main source of ionization, $H_3O^+ \cdot (H_2O)n$ is predominantly formed by the reaction paths (5) through (9) at all altitudes. NO^+ is formed through charge transfer at a faster rate than through Lyman-alpha ionization of NO so that NO^+ hydrates are still present at high concentrations. Increased electron densities and the comparatively greater efficiency of two-body electron-ion recombination as opposed to three-body hydrate formation at higher altitudes leads to a decrease of all types of hydrates above the mesopause for these disturbed conditions.

Negative Ions

Negative ions, according to current gas-phase chemistry, are formed through the interaction of electrons with the neutral species O_2, CO_2 and O_3, and are independent of the type or source of ionization. Their concentrations depend on the magnitude of the electron density, and the relative ratios are fairly constant despite the level of ionization, as Figs. 6 and 7 show. Therefore, a discussion of the negative ion formation and hydration processes for the quiet solar eclipse conditions will also be valid for disturbed conditions.

The negative ion chain is initiated by the three-body attachment of electrons to O_2

$$e + O_2 + M \rightarrow O_2^- + M \ . \qquad (10)$$

Dissociative attachment to O_3 also occurs

$$O_3 + e \rightarrow O^- + O_2 \ , \qquad (11)$$

but this is never a major "initial" source of negative ions in the mesosphere. Detachment occurs rapidly through

$$O_2^- + O \rightarrow O_3 + e \ , \qquad (12)$$

$$O_2^- + O_2(^1\Delta g) \rightarrow 2O_2 + e \ , \qquad (13)$$

$$O^- + X(N_2, O, H_2) \rightarrow OX + e \ . \qquad (14)$$

Photodetachment occurs also, but it is always slower than chemical means. The combination of a three-body formation process and two-body destruction processes, particularly with O, means that negative ions are never important in the upper mesosphere and only reach significant concentrations below 70 km.

The key to the buildup of appreciable negative ion concentrations is the reaction

$$O_2^- + O_3 \rightarrow O_3^- + O_2 \ , \qquad (15)$$

which is quickly followed by

$$O_3^- + CO_2 \rightarrow CO_3^- + O_2 \ . \qquad (16)$$

When reaction (15) dominates, the electrical charge can flow into the negative ions; when the detachment reactions (12) and (13) dominate, the electrical charge remains essentially as free electrons. The ratio of O/O_3 determines whether negative ions are formed or not. Allowing for differences in rate constants of reactions, plus the fact that $O_2(^1\Delta g)$ should also be included, one can use the rule of thumb that when $O/O_3 > 2$ electrons will dominate, and when $O/O_3 < 2$ negative ions will become appreciable or dominant.

Below 70 km, CO_3^- becomes the more prevalent negative ion with the balance gradually shifting to NO_3^- via the slow reactions

$$CO_3^- + NO \rightarrow NO_2^- + CO_2 \ , \qquad (17)$$

followed by

$$NO_2^- + O_3 \rightarrow NO_3^- + O_2 \ , \tag{18}$$

or the somewhat faster reaction

$$CO_3^- + NO_2 \rightarrow NO_3^- + CO_2 \ . \tag{19}$$

Although NO_3^- is formed rather slowly, it is also destroyed slowly and therefore builds up an appreciable concentration below 65 km. In the current negative ion scheme, NO_3^- is a terminal or "end-of-the-chain" ion. As rapidly as the sunlight disappears the CO_3^-, NO_3^- ions switch to their hydrates so that the hydrated ions dominate below 65 km near and during eclipse totality (Figs. 6, 9, 10, and 11).

COMPARISON WITH PREVIOUS MEASUREMENTS

Measurements of electron density from the 1966 solar eclipse are shown as dashed lines in Fig. 12 along with calculated electron densities at several altitudes for the 1979 eclipse. The contrasts are apparent. Experimental results show drops by factors of 4 to 10 in the 74 to 82 km region, while calculations show very little change anywhere above 70 km. The rapidity with which the decrease occurs in the experimental measurements cannot be matched in the calculated results.

For the calculated electron densities, 70 km appears to be the region where attachment processes occur which provide a decrease in electron density as seen at 65 km. In an attempt to determine the nature of these processes and to simulate the rapid changes observed in the 1966 eclipse, two classes of reactions are introduced. The first is an enhanced three-body attachment reaction

$$e + O_2 + X \rightarrow O_2^- + X \tag{20}$$

which provides more of the "initial" negative ion in the negative ion chain. The second class of reactions is an equivalent two-body attachment reaction

$$e + X \rightarrow Y + O_3^- \tag{21}$$

which essentially bypasses the formation of the initial negative ion O_2^- and provides an entry into the chain via O_3^-, which is quickly changed to CO_3^-.

The enhanced three-body attachment reaction is established by taking the normal reaction $e + O_2 + N_2 \rightarrow O_2^- + N_2$ (which nominally provides less than 25 percent of the total electron attachment) and increasing the rate constant two orders of magnitude so that it becomes the dominant

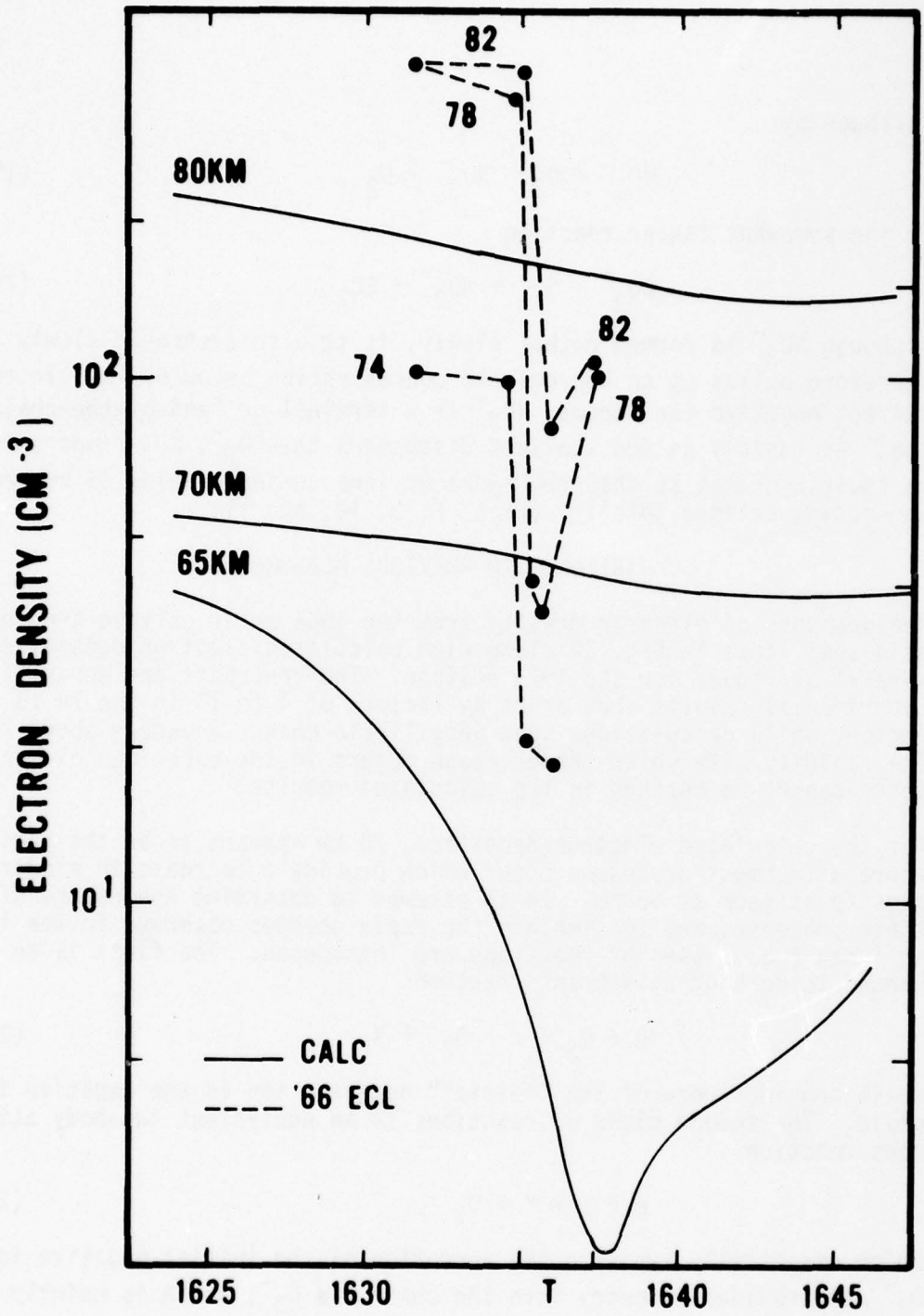

Figure 12. The time history of the calculated electron densities for the 1979 solar eclipse at 65, 70, and 80 km compared measured electron densities during the 1966 solar eclipse at 74, 78, and 82 km.

electron attachment process. The enhanced two-body attachment reaction is simulated by taking two reactions:

$$O_3 + e \rightarrow O^- + O_2 \qquad (11)$$

and

$$O^- + O_3 \rightarrow O_3^- + O \ , \qquad (12)$$

and increasing each of their rate constants two orders of magnitude so that they become the dominant equivalent electron attachment process.

These two types of enhanced attachment reactions are tried in order to provide a more rapid electron attachment mechanism and produce larger drops in the calculated electron densities, but still "preserve" the conventional gas phase negative ion chemistry. The results at 70 km for each of these classes of attachment reactions are shown in Fig. 13. While such enhanced pseudoreactions provide the desired overall drop in the electron density, the time sequence appears much too slow. Even worse, at 80 km the same classes of reactions produced no significant changes.

It is known, however, that large changes in the electron concentration do occur at 70 km in the day/night transition. The time sequence of density variations at sunset is compared with that of the eclipse in Fig. 14. Relatively large decreases in electron density occur rather rapidly at sunset, but do not occur during the eclipse because of the different densities of O and O_3 for the two cases. During the eclipse the O and O_3 densities (dashed lines in Fig. 14) approach each other, but the O_3 density never exceeds the O density. During sunset the O_3 density does exceed the O density (dot-dash lines) and thus allows the formation of more stable negative ions such as CO_3^-.

The flow of charge among the negative species during totality at 70 km is shown schematically in Fig. 15. The sequence of negative ion formation has been reviewed above in Eqs. (10) through (16). The crucial steps are having enough O_3 (in relation to O) to move the charge from O_2^- to O_3^- to CO_3^-, and then having a small enough amount of O so that the CO_3^- is not quickly destroyed through the reaction

$$CO_3^- + O \rightarrow O_2^- + CO_2 \ . \qquad (23)$$

Thus while it is possible to cause large changes in the 70 km region by the "conventional" negative ion chemistry through enhanced pseudoreactions, these mechanisms fail in the 80 km region due to the dominance of O and reactions (12) and (23). It has not been possible to even approximate the rapid changes shown in Fig. 12.

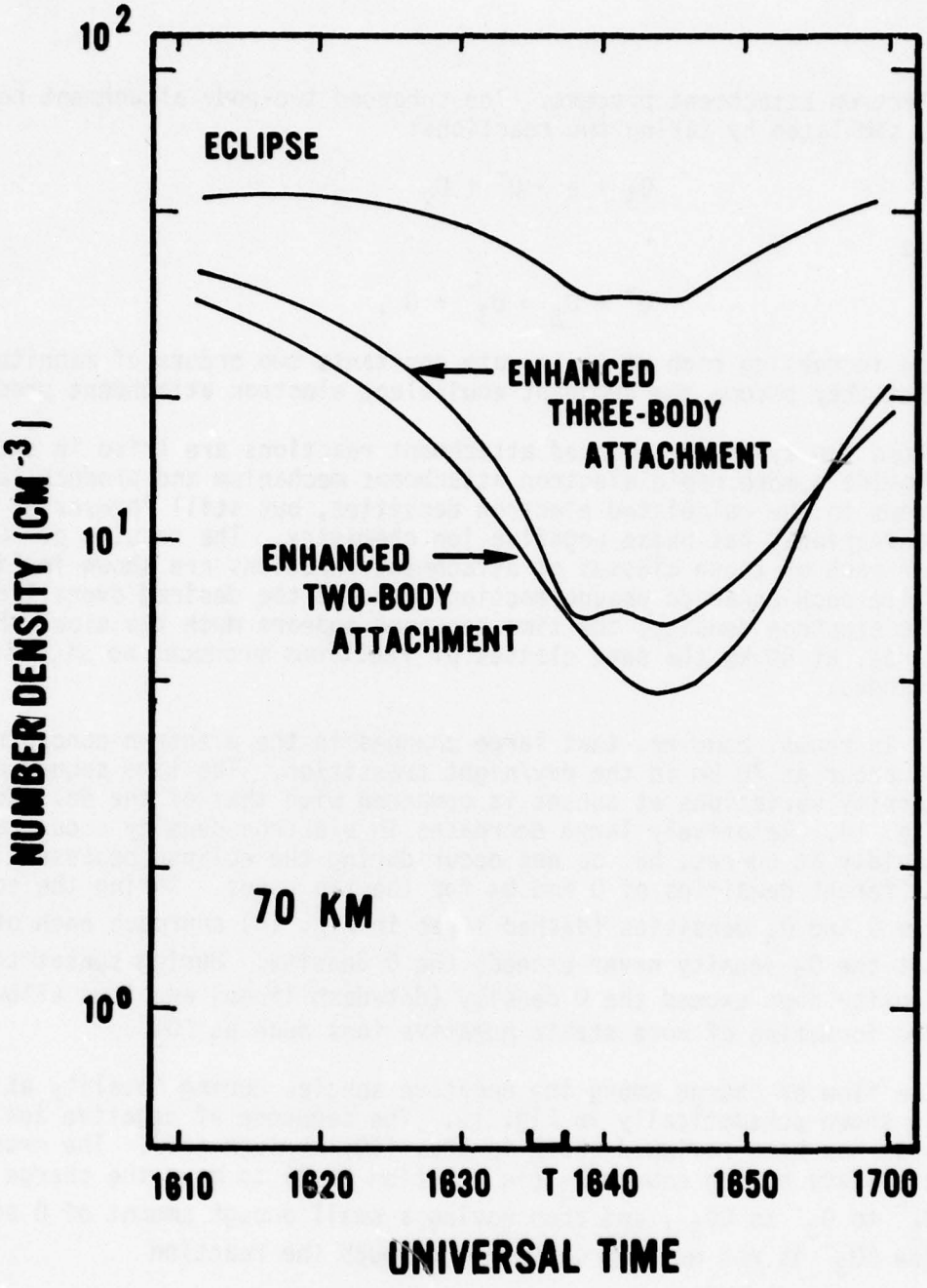

Figure 13. The time history of the electron density at 70 km during the eclipse. Also shown are two similar calculations for enhanced two-body and three-body attachment.

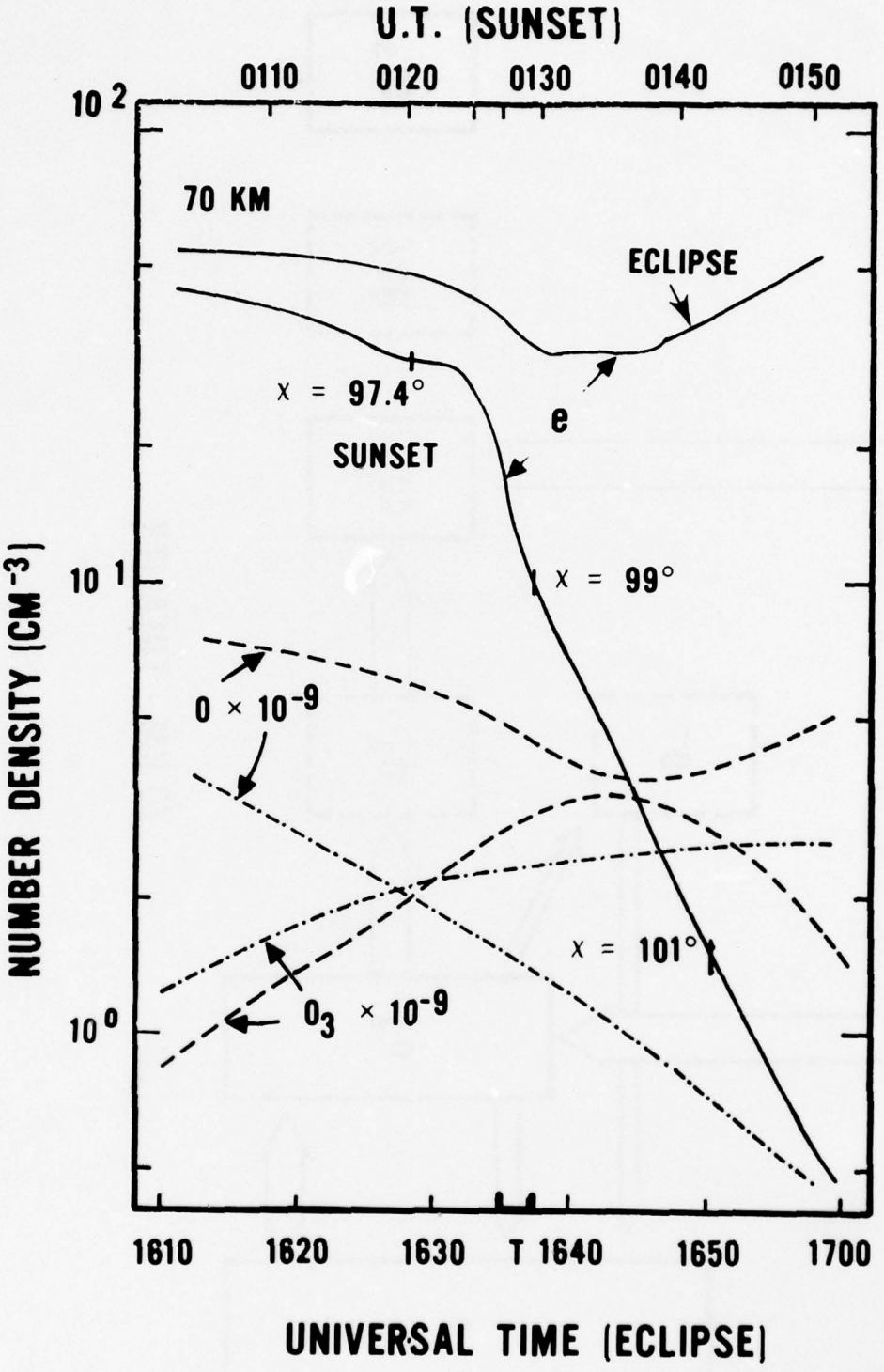

Figure 14. The time history of the electron densities at 70 km for the eclipse period and sunset later that day. Also shown are the O and O_3 densities during these same periods.

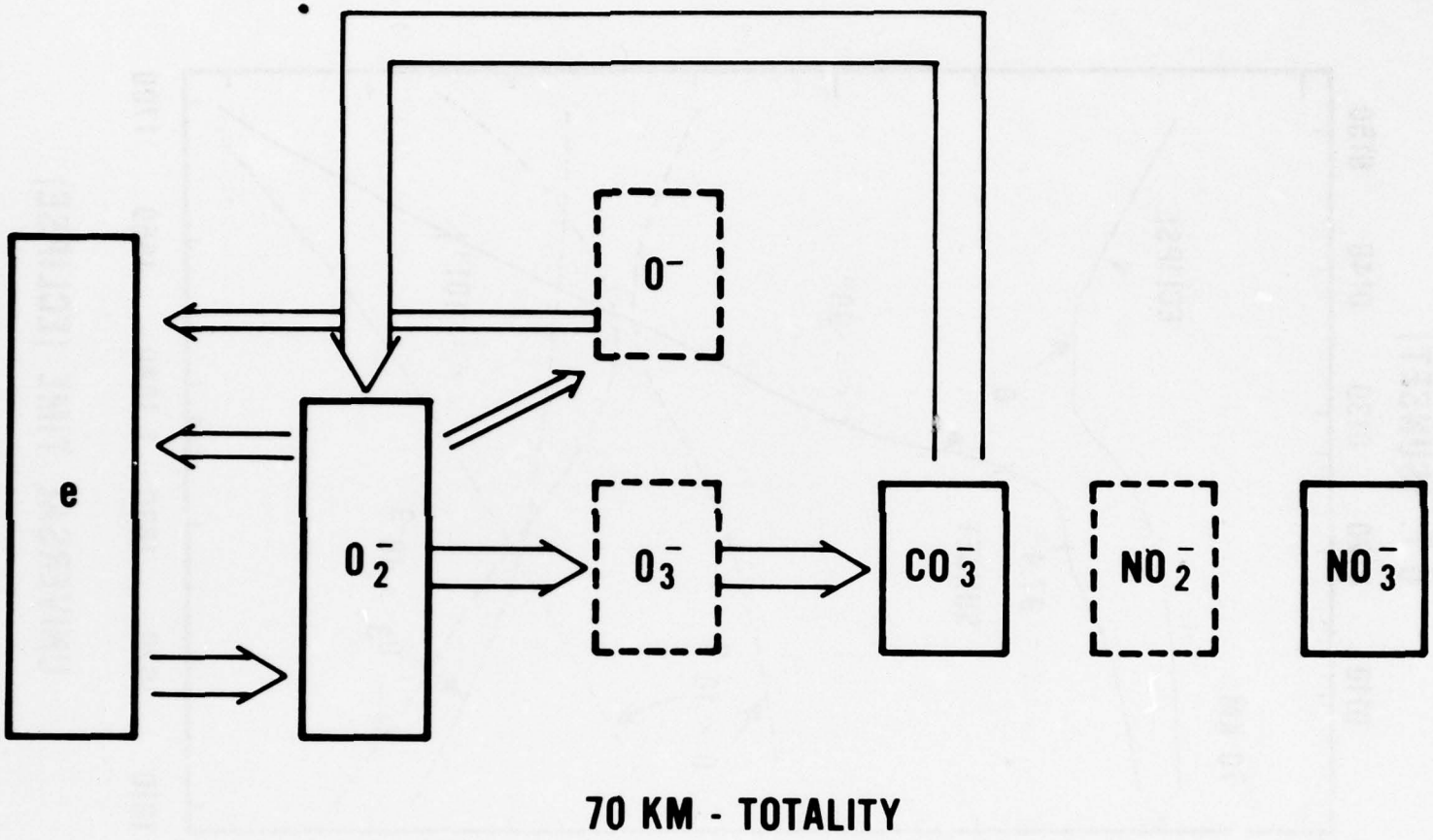

Figure 15. The flow of charge among the negative ion species at 70 km during totality.

Several other types of measurements made during solar eclipses are at odds with the results one would calculate using conventional gas-phase chemistry.

Different groups [4,5] have reported estimates of the effective recombination coefficient during eclipses ranging from 2-6 x 10^{-7} cm^3s^{-1} in the 90 to 95 km region to 5-10 x $10^{-5}cm^3s^{-1}$ near the 80 km. The effective recombination coefficient calculated for the 1979 eclipse is shown in Fig. 16. Reasonable agreement can be obtained above 90 km, but the calculated effective recombination coefficient is too small at 80 km. The large increase in the calculated coefficient below 70 km is due mainly to the greatly increased ratio of negative ions to electrons.

During the 1966 eclipse the total positive-ion density between 70 and 90 km was consistently measured to be greater than the electron density [6]. Calculations show this would not be the case until below 70 km. Positive ion hydrates have also been observed to decrease in the 70 to 90 km region during the eclipse [7]. This decrease does not occur below 85 km in these calculations.

Negative ions have been observed above 70 km on at least one occasion, with heavy negative particles (>150 amu) below 92 km [7]. The calculated results predict essentially no negative ions above 70 km.

CONCLUSIONS AND SUGGESTIONS

The current gas-phase chemistry is not capable of modeling the rapid changes in electron density observed during solar eclipses. New mechanisms must be sought which can provide for the rapid attachment and detachment of electrons which have been observed, as well as other "anomalous" features. Some broad outlines may be sketched as to what one might expect.

Particulates would be indicated whose number density, or at least mixing ratio, increases from the middle mesosphere to the mesopause and then decreases above the mesopause. This action would explain why the effects of the particulate or aerosol are apparently masked by the conventional three-body electron attachment chemistry below about 65 km, and why the conventional chemistry gives reasonable agreement above 90 km.

These particles should probably be capable of attaching positive ions as well as electrons. Such ion attachment may help explain classes of heavier charged particles with differing mobilities which are often measured.

The rapid variation in the observed electron densities in Fig. 12 would imply rapid attachment as well as rapid detachment of at least the electrons. The sharp drop-off of the electron densities indicates that this

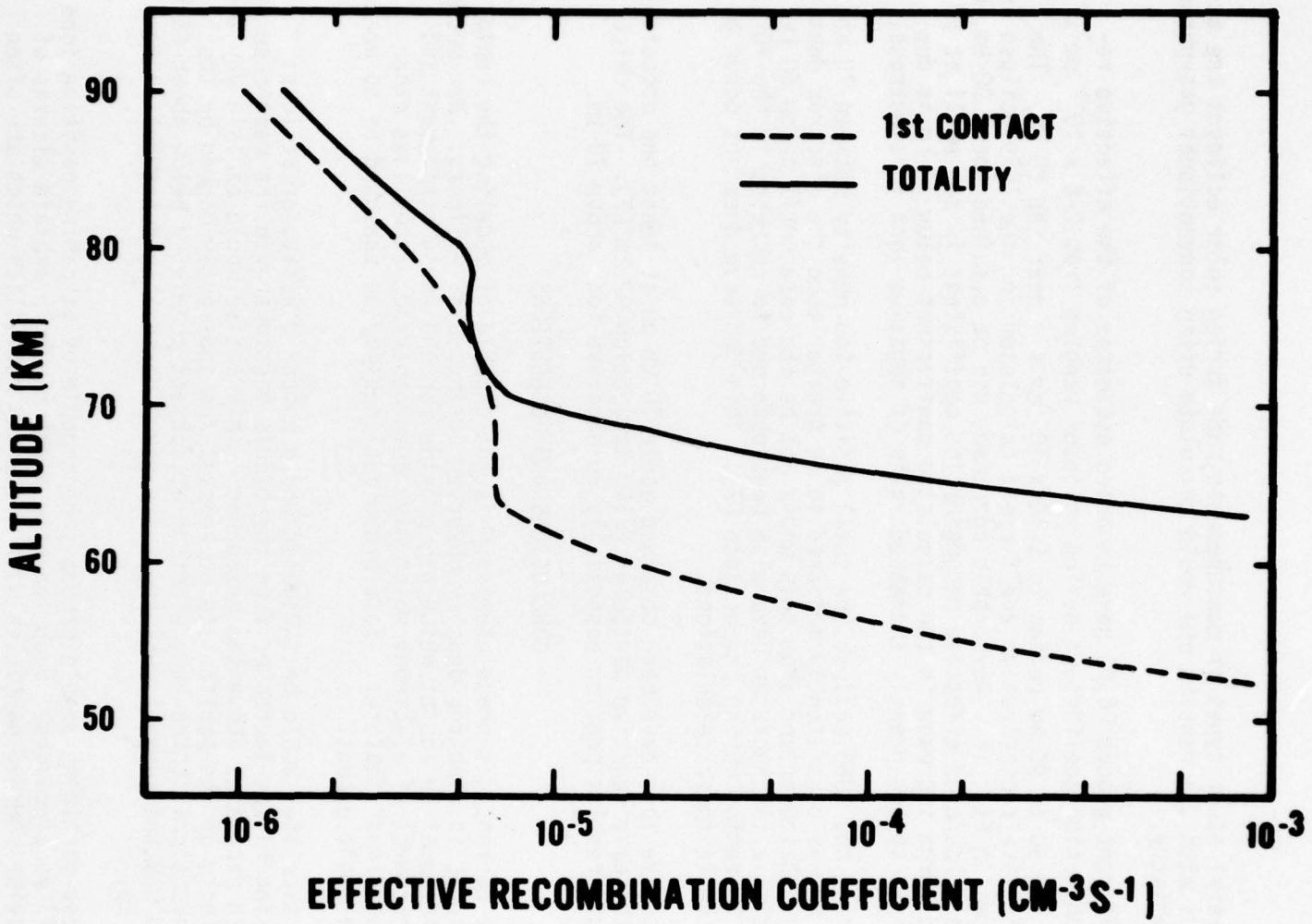

Figure 16. The effective recombination coefficient at first contact and again during totality.

class of particles would have an extremely large detachment cross section; consequently, the electron could not stay attached while there was light present and would immediately detach as soon as the solar disc became visible again. As soon as the solar disc is obscured, however, these same particles would very rapidly attach the available electrons (or a large fraction of them).

An extremely large photodetachment cross section could also account for the rapid drops being observed during the eclipse but not always during normal sunset-sunrise conditions. At higher altitudes, e.g., in the region of 80 km and above, the major source of ionization is Lyman-alpha radiation which is severely attenuated as the solar zenith angle increases past 85 degrees, almost an hour before the visible spectrum disappears. Therefore, the ambient electron density would decrease gradually through electron-ion recombination and would be at low enough levels by the time the visible light disappeared that attachment to particulates would no longer be the major loss process. Similarly, in the region around 70 km the electrons are able to advance along the negative ion chain due to the increase in ozone from the attenuation of ultraviolet light before the visible light is attenuated. Again the electrons have largely disappeared due to the "conventional" ion chemistry before the particulates are able to come into play. The fact that even during totality the electrons did not completely disappear (Fig. 12) would indicate that the number density of these particulates would be on the same order as the electrons, i.e., 10^2 - 10^4 cm^{-3}, so that as electrons began attaching to the particulates they would quickly saturate (assuming only one or a few electrons would attach per particulate), and the particulates would not be able to scavenge all the electrons that are available. Light scattering results indicate that a particle number density on the order of 10^2 - 10^4 cm^{-3} implies an extremely small size on the order of 0.01μ [8].

In conclusion, a growing body of measurements is pointing to a class of phenomena which are poorly understood but which definitely affect the ionization-deionization processes and total charge balance in the D-region of the atmosphere. The 1979 eclipse can serve as a focus to help determine what these phenomena are. A correct determination of D-region electron densities and electron attachment and detachment processes is necessary for proper utilization of Army communications systems and a better understanding of the effects of nuclear weapons in the middle atmosphere.

REFERENCES

1. Meira, L. G., Jr., 1971, "Rocket Measurements of Upper Atmospheric Nitric Oxide and Their Consequences to the Lower Ionosphere," J. Geophys. Res., 76:202-212.

2. Ogawa, T., and T. Shimazaki, 1975, "Diurnal Variations of Odd Nitrogen and Ionic Densities in the Mesosphere and Lower Thermosphere: Simultaneous Solution of Photochemical-Diffusive Equations," J. Geophys. Res., 80:3945-3960.

3. Heaps, M. G., 1976, "Synopsis of Ionization Sources in the Mesosphere and Stratosphere, with Particular Emphasis Given to the Path of the 26 February 1979 Solar Eclipse," BRL Report No. 1938, US Army Ballistic Research Laboratories.

4. Mechtly, E. A., C. F. Sechrist, Jr., and L. G. Smith, 1972, "Effective Loss Coefficients for the D-Region of the Ionosphere from Rocket Measurements During the Eclipses of March 1970 and November 1966," J. Atmospheric Terrest. Phys., 34:641-646.

5. Belrose, J. S., D. B. Ross, and A. G. McNamara, 1972, "Ionization Changes in the Lower Ionosphere During the Solar Eclipse of 7 March 1970," J. Atmospheric Terrest. Phys., 34:627-640.

6. Sears, R. D., 1972, "Analysis of the 1966 Solar Eclipse Data," LSMC D246526, Lockheed Palo Alto Research Laboratory.

7. Narcisi, R. S., A. D. Bailey, L. E. Wlodyka, and C. R. Philbrick, 1972, "Ion Composition in the Lower Ionosphere During the November 1966 and March 1970 Eclipses," J. Atmospheric Terrest. Phys., 34:647-658.

8. Hale, L. C., 1977, "Particulate Transport Through the Mesosphere and Stratosphere," EOS, Trans. Am. Geophys. Union, 58:695.

APPENDIX

TYPES OF MEASUREMENTS NEEDED

Neutral gas density profile

Temperature profile

O_3 density

O density

NO density

H_2O density

Precipitating particle fluxes and energy spectrum

In situ ion-pair production rate measurements

Electron densities, frequent measurements before, during, and after totality

Positive ion measurements

Negative ion measurements

Conductivity measurements

Solar flux variations in

- x-rays
- Lyman-alpha
- ultraviolet
- visible

DISTRIBUTION LIST

Director
US Army Ballistic Research Laboratory
ATTN: DRDAR-BLB, Dr. G. E. Keller
Aberdeen Proving Ground, MD 21005

Air Force Weapons Laboratory
ATTN: Technical Library (SUL)
Kirtland AFB, NM 87117

Commander
Headquarters, Fort Huachuca
ATTN: Tech Ref Div
Fort Huachuca, AZ 85613

6585 TG/WE
Holloman AFB, NM 88330

Commandant
US Army Field Artillery School
ATTN: Morris Swett Tech Library
Fort Sill, OK 73503

Commandant
USAFAS
ATTN: ATSF-CD-MT (Mr. Farmer)
Fort Sill, OK 73503

Director
US Army Engr Waterways Exper Sta
ATTN: Library Branch
Vicksburg, MS 39180

Commander
US Army Electronics Command
ATTN: DRSEL-CT-S (Dr. Swingle)
Fort Monmouth, NJ 07703
03

CPT Hugh Albers, Exec Sec
Interdept Committee on Atmos Sci
Fed Council for Sci & Tech
National Sci Foundation
Washington, DC 20550

Inge Dirmhirn, Professor
Utah State University, UMC 48
Logan, UT 84322

HQDA (DAEN-RDM/Dr. De Percin)
Forrestal Bldg
Washington, DC 20314

Commander
US Army Aviation Center
ATTN: ATZQ-D-MA
Fort Rucker, AL 36362

CO, USA Foreign Sci & Tech Center
ATTN: DRXST-ISI
220 7th Street, NE
Charlottesville, VA 22901

Director
USAE Waterways Experiment Station
ATTN: Library
PO Box 631
Vicksburg, MS 39180

US Army Research Office
ATTN: DRXRO-IP
PO Box 12211
Research Triangle Park, NC 27709

Mr. William A. Main
USDA Forest Service
1407 S. Harrison Road
East Lansing, MI 48823

Library-R-51-Tech Reports
Environmental Research Labs
NOAA
Boulder, CO 80302

Commander
US Army Dugway Proving Ground
ATTN: MT-S
Dugway, UT 84022

HQ, ESD/DRI/S-22
Hanscom AFB
MA 01731

Head, Atmospheric Rsch Section
National Science Foundation
1800 G. Street, NW
Washington, DC 20550

Office, Asst Sec Army (R&D)
ATTN: Dep for Science & Tech
HQ, Department of the Army
Washington, DC 20310

Commander
US Army Satellite Comm Agc
ATTN: DRCPM-SC-3
Fort Monmouth, NJ 07703

Sylvania Elec Sys Western Div
ATTN: Technical Reports Library
PO Box 205
Mountain View, CA 94040

William Peterson
Research Association
Utah State University, UNC 48
Logan, UT 84322

Defense Communications Agency
Technical Library Center
Code 205
Washington, DC 20305

Dr. A. D. Belmont
Research Division
PO Box 1249
Control Data Corp
Minneapolis, MN 55440

Commander
US Army Electronics Command
ATTN: DRSEL-WL-D1
Fort Monmouth, NJ 07703

Commander
ATTN: DRSEL-VL-D
Fort Monmouth, NJ 07703

Meteorologist in Charge
Kwajalein Missile Range
PO Box 67
APO
San Francisco, CA 96555

The Library of Congress
ATTN: Exchange & Gift Div
Washington, DC 20540
2

US Army Liaison Office
MIT-Lincoln Lab, Library A-082
PO Box 73
Lexington, MA 02173

Dir National Security Agency
ATTN: TDL (C513)
Fort George G. Meade, MD 20755

Director, Systems R&D Service
Federal Aviation Administration
ATTN: ARD-54
2100 Second Street, SW
Washington, DC 20590

Commander
US Army Missile Command
ATTN: DRSMI-RRA, Bldg 7770
Redstone Arsenal, AL 35809

Dir of Dev & Engr
Defense Systems Div
ATTN: SAREA-DE-DDR
H. Tannenbaum
Edgewood Arsenal, APG, MD 21010

Naval Surface Weapons Center
Technical Library & Information
Services Division
White Oak, Silver Spring, MD
20910

Dr. Frank D. Eaton
PO Box 3038
Universtiy Station
Laramie, Wyoming 82071

Rome Air Development Center
ATTN: Documents Library
TILD (Bette Smith)
Griffiss Air Force Base, NY 13441

National Weather Service
National Meteorological Center
World Weather Bldg - 5200 Auth Rd
ATTN: Mr. Quiroz
Washington, DC 20233

USAFETAC/CB (Stop 825)
Scott AFB
IL 62225

Director
Defense Nuclear Agency
ATTN: Tech Library
Washington, DC 20305

Director
Development Center MCDEC
ATTN: Firepower Division
Quantico, VA 22134

Environmental Protection Agency
Meteorology Laboratory
Research Triangle Park, NC
27711

Commander
US Army Electronics Command
ATTN: DRSEL-GG-TD
Fort Monmouth, NJ 07703

Commander
US Army Ballistic Rsch Labs
ATTN: DRXBR-IB
APG, MD 21005

Dir, US Naval Research Lab
Code 5530
Washington, DC 20375

Mil Assistant for
Environmental Sciences
DAD (E & LS), 3D129
The Pentagon
Washington, DC 20301

The Environmental Rsch
Institute of MI
ATTN: IRIA Library
PO Box 618
Ann Arbor, MI 48107

Armament Dev & Test Center
ADTC (DLOSL)
Eglin AFB, Florida 32542

Range Commanders Council
ATTN: Mr. Hixon
PMTC Code 3252
Pacific Missile Test Center
Point Mugu, CA 93042

Commander
Eustis Directorate
US Army Air Mobility R&D Lab
ATTN: Technical Library
Fort Eustis, VA 23604

Commander
Frankford Arsenal
ATTN: SARFA-FCD-O, Bldg 201-2
Bridge & Tarcony Sts
Philadelphia, PA 19137

Director, Naval Oceanography and
Meteorology
National Space Technology Laboratories
Bay St Louis, MS 39529

Commander
US Army Electronics Command
ATTN: DRSEL-CT-S
Fort Monmouth, NJ 07703

Commander
USA Cold Regions Test Center
ATTN: STECR-OP-PM
APO Seattle 98733

Redstone Scientific Information Center
ATTN: DRDMI-TBD
US Army Missile Res & Dev Command
Redstone Arsenal, AL 35809

Commander
AFWL/WE
Kirtland AFB, NM 87117

Naval Surface Weapons Center
Code DT-22 (Ms. Greeley)
Dahlgren, VA 22448

Commander
Naval Ocean Systems Center
ATTN: Research Library
San Diego, CA 92152

Commander
US Army INSCOM
ATTN: IARDA-OS
Arlington Hall Station
Arlington, VA 22212

Commandant
US Army Field Artillery School
ATTN: ATSF-CF-R
Fort Sill, OK 73503

Commander and Director
US Army Engineer Topographic Labs
ETL-GS-AC
Fort Belvoir, VA 22060

Technical Processes Br-D823
NOAA, Lib & Info Serv Div
6009 Executive Blvd
Rockville, MD 20852

Commander
US Army Missile Research
and Development Command
ATTN: DRDMI-CGA, B. W. Fowler
Redstone Arsenal, AL 35809

Commanding Officer
US Army Armament Rsch & Dev Com
ATTN: DRDAR-TSS #59
Dover, NJ 07801

Air Force Cambridge Rsch Labs
ATTN: LCB (A. S. Carten, Jr.)
Hanscom AFB
Bedford, MA 01731

National Center for Atmos Res
NCAR Library
PO Box 3000
Boulder, CO 80307

Air Force Geophysics Laboratory
ATTN: LYD
Hanscom AFB
Bedford, MA 01731

Chief, Atmospheric Sciences Division
Code ES-81
NASA
Marshall Space Flight Center, AL 35812

Department of the Air Force
OL-C, 5WW
Fort Monroe, VA 23651

Commander
US Army Missile Rsch & Dev Com
ATTN: DRDMI-TR
Redstone Arsenal, AL 35809

Meteorology Laboratory
AFGL/LY
Hanscom AFB, MA 01731

Director CFD
US Army Field Artillery School
ATTN: Met Division
Fort Sill, OK 73503

Naval Weapons Center (Code 3173)
ATTN: Dr. A. Shlanta
China Lake, CA 93555

Director
Atmospheric Physics & Chem Lab
Code R31, NOAA
Department of Commerce
Boulder, CO 80302

Department of the Air Force
5 WW/DN
Langley AFB, VA 23665

Commander
US Army Intelligence Center and School
ATTN: ATSI-CD-MD
Fort Huachuca, AZ 85613

Dr. John L. Walsh
Code 4109
Navy Research Lab
Washington, DC 20375

Director
US Army Armament Rsch & Dev Com
Chemical Systems Laboratory
ATTN: DRDAR-CLJ-I
Aberdeen Proving Ground, MD 21010

R. B. Girardo
Bureau of Reclamation
E&R Center, Code 1220
Denver Federal Center, Bldg 67
Denver, CO 80225

Commander
US Army Missile Command
ATTN: DRDMI-TEM
Redstone Arsenal, AL 35809

Commander
US Army Tropic Test Center
ATTN: STETC-MO (Tech Library)
APO New York 09827

Commanding Officer
Naval Research Laboratory
Code 2627
Washington, DC 20375

Defense Documentation Center
ATTN: DDC-TCA
Cameron Station (Bldg 5)
Alexandria, Virginia 22314
12

Commander
US Army Test and Evaluation Command
ATTN: Technical Library
White Sands Missile Range, NM 88002

US Army Nuclear Agency
ATTN: MONA-WE
Fort Belvoir, VA 22060

Commander
US Army Proving Ground
ATTN: Technical Library
Bldg 2100
Yuma, AZ 85364

Office, Asst Sec Army (R&D)
ATTN: Dep for Science & Tech
HQ, Department of the Army
Washington, DC 20310

ATMOSPHERIC SCIENCES RESEARCH PAPERS

1. Lindberg, J.D., "An Improvement to a Method for Measuring the Absorption Coefficient of Atmospheric Dust and other Strongly Absorbing Powders, " ECOM-5565, July 1975.
2. Avara, Elton, P., "Mesoscale Wind Shears Derived from Thermal Winds," ECOM-5566, July 1975.
3. Gomez, Richard B., and Joseph H. Pierluissi, "Incomplete Gamma Function Approximation for King's Strong-Line Transmittance Model," ECOM-5567, July 1975.
4. Blanco, A.J., and B.F. Engebos, "Ballistic Wind Weighting Functions for Tank Projectiles," ECOM-5568, August 1975.
5. Taylor, Fredrick J., Jack Smith, and Thomas H. Pries, "Crosswind Measurements through Pattern Recognition Techniques," ECOM-5569, July 1975.
6. Walters, D.L., "Crosswind Weighting Functions for Direct-Fire Projectiles," ECOM-5570, August 1975.
7. Duncan, Louis D., "An Improved Algorithm for the Iterated Minimal Information Solution for Remote Sounding of Temperature," ECOM-5571, August 1975.
8. Robbiani, Raymond L., "Tactical Field Demonstration of Mobile Weather Radar Set AN/TPS-41 at Fort Rucker, Alabama," ECOM-5572, August 1975.
9. Miers, B., G. Blackman, D. Langer, and N. Lorimier, "Analysis of SMS/GOES Film Data," ECOM-5573, September 1975.
10. Manquero, Carlos, Louis Duncan, and Rufus Bruce, "An Indication from Satellite Measurements of Atmospheric CO2 Variability," ECOM-5574, September 1975.
11. Petracca, Carmine, and James D. Lindberg, "Installation and Operation of an Atmospheric Particulate Collector," ECOM-5575, September 1975.
12. Avara, Elton P., and George Alexander, "Empirical Investigation of Three Iterative Methods for Inverting the Radiative Transfer Equation," ECOM-5576, October 1975.
13. Alexander, George D., "A Digital Data Acquisition Interface for the SMS Direct Readout Ground Station — Concept and Preliminary Design," ECOM-5577, October 1975.
14. Cantor, Israel, "Enhancement of Point Source Thermal Radiation Under Clouds in a Nonattenuating Medium," ECOM-5578, October 1975.
15. Norton, Colburn, and Glenn Hoidale, "The Diurnal Variation of Mixing Height by Month over White Sands Missile Range, N.M," ECOM-5579, November 1975.
16. Avara, Elton P., "On the Spectrum Analysis of Binary Data," ECOM-5580, November 1975.
17. Taylor, Fredrick J., Thomas H. Pries, and Chao-Huan Huang, "Optimal Wind Velocity Estimation," ECOM-5581, December 1975.
18. Avara, Elton P., "Some Effects of Autocorrelated and Cross-Correlated Noise on the Analysis of Variance, " ECOM-5582, December 1975.
19. Gillespie, Patti S., R.L. Armstrong, and Kenneth O. White, "The Spectral Characteristics and Atmospheric CO2 Absorption of the Ho^{+3}:YLF Laser at 2.05μm," ECOM-5583, December 1975.
20. Novlan, David J. "An Empirical Method of Forecasting Thunderstorms for the White Sands Missile Range," ECOM-5584, February 1976.
21. Avara, Elton P.. "Randomization Effects in Hypothesis Testing with Autocorrelated Noise," ECOM-5585, February 1976.
22. Watkins, Wendell R., "Improvements in Long Path Absorption Cell Measurement," ECOM-5586, March 1976.
23. Thomas, Joe, George D. Alexander, and Marvin Dubbin, "SATTEL — An Army Dedicated Meteorological Telemetry System," ECOM-5587. March 1976.
24. Kennedy, Bruce W., and Delbert Bynum, "Army User Test Program for the RDT&E-XM-75 Meteorological Rocket," ECOM-5588, April 1976.

25. Barnett, Kenneth M., "A Description of the Artillery Meteorological Comparisons at White Sands Missle Range, October 1974 - December 1974 ('PASS' - Prototype Artillery [Meteorological] Subsystem)," ECOM-5589, April 1976.
26. Miller, Walter B., "Preliminary Analysis of Fall-of-Shot From Project 'PASS'," ECOM-5590, April 1976.
27. Avara, Elton P., "Error Analysis of Minimum Information and Smith's Direct Methods for Inverting the Radiative Transfer Equation," ECOM-5591, April 1976.
28. Yee, Young P., James D. Horn, and George Alexander, "Synoptic Thermal Wind Calculations from Radiosonde Observations Over the Southwestern United States," ECOM-5592, May 1976.
29. Duncan, Louis D., and Mary Ann Seagraves, "Applications of Empirical Corrections to NOAA-4 VTPR Observations," ECOM-5593, May 1976.
30. Miers, Bruce T., and Steve Weaver, "Applications of Meterological Satellite Data to Weather Sensitive Army Operations,"ECOM-5594, May 1976.
31. Sharenow, Moses, "Redesign and Improvement of Balloon ML-566," ECOM-5595, June, 1976.
32. Hansen, Frank V., "The Depth of the Surface Boundary Layer," ECOM-5596, June 1976.
33. Pinnick, R.G., and E.B. Stenmark, "Response Calculations for a Commercial Light-Scattering Aerosol Counter," ECOM-5597, July 1976.
34. Mason, J., and G.B. Hoidale, "Visibility as an Estimator of Infrared Transmittance," ECOM-5598, July 1976.
35. Bruce, Rufus E., Louis D. Duncan, and Joseph H. Pierluissi, "Experimental Study of the Relationship Between Radiosonde Temperatures and Radiometric-Area Temperatures," ECOM-5599, August 1976.
36. Duncan, Louis D., "Stratospheric Wind Shear Computed from Satellite Thermal Sounder Measurements," ECOM-5800, September 1976.
37. Taylor, F., P. Mohan, P. Joseph and T. Pries, "An All Digital Automated Wind Measurement System," ECOM-5801, September 1976.
38. Bruce, Charles, "Development of Spectrophones for CW and Pulsed Radiation Sources," ECOM-5802, September 1976.
39. Duncan, Louis D., and Mary Ann Seagraves,"Another Method for Estimating Clear Column Radiances," ECOM-5803, October 1976.
40. Blanco, Abel J., and Larry E. Taylor, "Artillery Meteorological Analysis of Project Pass," ECOM-5804, October 1976.
41. Miller, Walter, and Bernard Engebos," A Mathematical Structure for Refinement of Sound Ranging Estimates," ECOM-5805, November, 1976.
42. Gillespie, James B., and James D. Lindberg, "A Method to Obtain Diffuse Reflectance Measurements from 1.0 to 3.0 μm Using a Cary 17I Spectrophotometer," ECOM-5806, November 1976.
43. Rubio, Roberto, and Robert O. Olsen,"A Study of the Effects of Temperature Variations on Radio Wave Absorption,"ECOM-5807, November 1976.
44. Ballard, Harold N., "Temperature Measurements in the Stratosphere from Balloon-Borne Instrument Platforms, 1968-1975," ECOM-5808, December 1976.
45. Monahan, H.H., "An Approach to the Short-Range Prediction of Early Morning Radiation Fog," ECOM-5809, January 1977.
46. Engebos, Bernard Francis, "Introduction to Multiple State Multiple Action Decision Theory and Its Relation to Mixing Structures," ECOM-5810, January 1977.
47. Low, Richard D.H.,"Effects of Cloud Particles on Remote Sensing from Space in the 10-Micrometer Infrared Region," ECOM-5811, January 1977.
48. Bonner, Robert S., and R. Newton, "Application of the AN/GVS-5 Laser Rangefinder to Cloud Base Height Measurements," ECOM-5812, February 1977.
49. Rubio, Roberto, "Lidar Detection of Subvisible Reentry Vehicle Erosive Atmospheric Material," ECOM-5813, March 1977.
50. Low, Richard D.H., and J.D. Horn, "Mesoscale Determination of Cloud-Top Height: Problems and Solutions," ECOM-5814, March 1977.

51. Duncan, Louis D., and Mary Ann Seagraves, "Evaluation of the NOAA-4 VTPR Thermal Winds for Nuclear Fallout Predictions," ECOM-5815, March 1977.
52. Randhawa, Jagir S., M. Izquierdo, Carlos McDonald and Zvi Salpeter, "Stratospheric Ozone Density as Measured by a Chemiluminescent Sensor During the Stratcom VI-A Flight," ECOM-5816, April 1977.
53. Rubio, Roberto, and Mike Izquierdo, "Measurements of Net Atmospheric Irradiance in the 0.7- to 2.8-Micrometer Infrared Region," ECOM-5817, May 1977.
54. Ballard, Harold N., Jose M. Serna, and Frank P. Hudson Consultant for Chemical Kinetics, "Calculation of Selected Atmospheric Composition Parameters for the Mid-Latitude, September Stratosphere," ECOM-5818, May 1977.
55. Mitchell, J.D., R.S. Sagar, and R.O. Olsen, "Positive Ions in the Middle Atmosphere During Sunrise Conditions," ECOM-5819, May 1977.
56. White, Kenneth O., Wendell R. Watkins, Stuart A. Schleusener, and Ronald L. Johnson, "Solid-State Laser Wavelength Identification Using a Reference Absorber," ECOM-5820, June 1977.
57. Watkins, Wendell R., and Richard G. Dixon, "Automation of Long-Path Absorption Cell Measurements," ECOM-5821, June 1977.
58. Taylor, S.E., J.M. Davis, and J.B. Mason, "Analysis of Observed Soil Skin Moisture Effects on Reflectance," ECOM-5822, June 1977.
59. Duncan, Louis D. and Mary Ann Seagraves, "Fallout Predictions Computed from Satellite Derived Winds," ECOM-5823, June 1977.
60. Snider, D.E., D.G. Murcray, F.H. Murcray, and W.J. Williams, "Investigation of High-Altitude Enhanced Infrared Backround Emissions" (U), SECRET, ECOM-5824, June 1977.
61. Dubbin, Marvin H. and Dennis Hall, "Synchronous Meteorlogical Satellite Direct Readout Ground System Digital Video Electronics," ECOM-5825, June 1977.
62. Miller, W., and B. Engebos, "A Preliminary Analysis of Two Sound Ranging Algorithms," ECOM-5826, July 1977.
63. Kennedy, Bruce W., and James K. Luers, "Ballistic Sphere Techniques for Measuring Atomspheric Parameters," ECOM-5827, July 1977.
64. Duncan, Louis D., "Zenith Angle Variation of Satellite Thermal Sounder Measurements," ECOM-5828, August 1977.
65. Hansen, Frank V., "The Critical Richardson Number," ECOM-5829, September 1977.
66. Ballard, Harold N., and Frank P. Hudson (Compilers), "Stratospheric Composition Balloon-Borne Experiment," ECOM-5830, October 1977.
67. Barr, William C., and Arnold C. Peterson, "Wind Measuring Accuracy Test of Meteorological Systems," ECOM-5831, November 1977.
68. Ethridge, G.A. and F.V. Hansen, "Atmospheric Diffusion: Similarity Theory and Empirical Derivations for Use in Boundary Layer Diffusion Problems," ECOM-5832, November 1977.
69. Low, Richard D.H., "The Internal Cloud Radiation Field and a Technique for Determining Cloud Blackness," ECOM-5833, December 1977.
70. Watkins, Wendell R., Kenneth O. White, Charles W. Bruce, Donald L. Walters, and James D. Lindberg, "Measurements Required for Prediction of High Energy Laser Transmission," ECOM-5834, December 1977.
71. Rubio, Robert, "Investigation of Abrupt Decreases in Atmospherically Backscattered Laser Energy," ECOM-5835, December 1977.
72. Monahan, H.H. and R.M. Cionco, "An Interpretative Review of Existing Capabilities for Measuring and Forecasting Selected Weather Variables (Emphasizing Remote Means)," ASL-TR-0001, January 1978.
73. Heaps, Melvin G., "The 1979 Solar Eclipse and Validation of D-Region Models," ASL-TR-0002. March 1978.

☆ U.S. GOVERNMENT PRINTING OFFICE: 1977 777-093/34